Republic of Iraq
Ministry of Higher Education and Scientific Research
University of Babylon
College of Science for Women
Department of Chemistry

Hydrothermal Synthesis Cr_2O_3\ZnO Nanocomposite for Enviromantal Applications

A Thesis Submitted to the Council of the College of Science for women, University of Babylon as a Partial Fulfillment of the Requirements for the Degree of Mas-ter, in Chemistry

by

Karam Kadhim Abd zaid

B.Sc., Chemistry of Science, University of Babylon College of Sci-ences for Women (2019-2020)

Supervised by

Prof. Dr. Hazim Yahya Algubury

1444 A.H **2023 A.D**

بسم الله الرحمن الرحيم

(بَلْ هُوَ آيَاتٌ بَيِّنَاتٌ فِي صُدُورِ الَّذِينَ أُوتُوا الْعِلْمَ وَمَا يَجْحَدُ بِآيَاتِنَا إِلَّا الظَّالِمُونَ).

صدق الله العلي العظيم

سورة العنكبوت، آية 49

Certification

I certify that this thesis entitled " **Hydrothermal synthesis of Cr_2O_3\ZnO Nanocomposite for enviromantal application** " was prepared under my supervision at the Department of Chemistry, College of Science for Women, Babylon University, in partial reqirements for the degree of Master of science in chemistry.

Signature:
Name: **Dr. Hazim Yahya Mohammed Ali**
Title: Professor
Date: \ \ 2023

In the view of the available recommendation, I forward this thesis for debate by the Examination Committee.

Signature:
Name: **Dr. Sadiq Abd AL-Hussein Karim**
Title: Professor
Address: Head of Department of Chemistry, College of Science for women, Babylon University
Date: \ \ 2023

Dedication

I dedicate this work to the face of Allah (Glory be upon Him)

To my parents the source of my strength

To my beautiful sisters and brothers

To my husband and to my little Prince Youssef

To everyone who believes in me

Karam

Acknowledgements

My first thinks go to Allah (Glory be upon him) who enabled me to realize my first dream. I extend my sincere thanks to my supervisor Prof., Dr. Hazim Yahya Al-gubury for the proposal, guidance and assistance he provided in carrying out this work, it was an honor to be one of his students Sincere thanks are due to the Prof. Dr. Ayad Alkaim, for their help in this work.

All thanks to the professors of the Department of Chemistry.

All thanks to my family, friends and colleagues for the support and encouragement.

karam

This work contains two major parts :

1-The first part includes preparation of zinc oxide (ZnO) nanopartical by and Cr_2O_3/ZnO nanocomposite by hydrothermal method. Study the characteristic of nanocomposite using various techniques such as X-ray diffraction (XRD), Fourier transform infrared (FTIR), Scanning electron microscopy (SEM), and Thermo gravimetric analysis (TGA). The particle size of synthesized Cr_2O_3/ZnO nanocomposite was calculate using scherer equation (12.74nm).

2-The second part include study of photo catalytic activity of prepared nanocomposite, by using acid fuchsin dye. The rate of photocatalytic degradation process is affected by different parameters such as initial concentration of dye, effect of mass of catalyst, initial pH of solution, effect of temperature, effect of scavenger, and effect of hydrogen peroxide.

Activation energy for the photo degradation process was calculated using arrhenius equation. they were equal to (31.67 KJ/mol). Enthalpy and entropy of activation and free energy of activation can be estimated according to eyring equation. Thermodynamic parameters (ΔH, ΔSand ΔG) for acid fuchsin dye were calculated (29.20 kJ/mol, - 0.1778 kJ/mol. k, and 82.18 kJ/mol respectively, from the results the reaction is endothermic with low randomness. ΔG (81.75 kJ/mol) was calculated and the reaction is non-spontaneous.

Table of Contents

Cuntents

Cuntents

Contents

Chapter Three: Results and Discussion

Contents

Contents

List of Tables

Chapter two: Experimental Part

Chapter Three: Results and Discussion

Contents

List of Figures

Chapter One: Introduction

Contents

Chapter Two: Experimental Part

Chapter Three: Results and Discussion

Contents

Contents

List of Abbreviations

Abbreviation	Description
Å	Angstrom
Atm	Atmosphere
Abs	Absorbance
BET	Brauner Emeet Teller
C	Concentration
Cal	Calculated
C_B	Conduction band
$^{\circ}C$	Centigrade
cm	Centimeter
Comm.	Commercial
CVD	Chemical Vapor Deposition
DI-H_2O	Deionized water
D.W	Distal water
Eg	Energy gap
e^{-}_{CB}	Negative electron conduction band
Etc	et cetera
Exp	Experimental
Eq	Equation
SEM	Scanning Electron Microscopy
FTIR	Fourier Transform Infrared Spectroscopy
G	Gram
h^{+}_{VB}	Positive hole valance band
K	Kelvin
Log	Logarithm
mA	Milliampere

Mg	Milligram
Min	Minute
Ml	Milliliter
MPa.	Mega pascal
Mw	Milliwatt
Nm	Nanometer
NMs	Nanomaterial
NPs	Nanoparticles
Ppm	Part per million
Pre.	Prepard
PVS	physical vapor synthesis
T	Temperature
T	Time
UV	Ultraviolet
UV–vis	Ultraviolet–visible
V	Volume
VB	Valance band
W	Weight
XRD	X-ray diffraction
ZnO NPs	Zinc Oxide Nanoparticles
hν	The photon energy
Hv	Wavelength
K	Adsorption rate constant
Θ	Bragg's angle of the peak
B	Full width at half- maximum intensity of the diffraction peaks
ω	Frequency
$e^{-}\backslash h^{+}$ pair	Electron- hole pair
D	Average crystal size
PDE	Photo degrade efficient
AOPS	Advance oxidation processes
FCc	Face centred cubic
HCp	Hexagonal closed pack
ROS	Reactive oxygen species
JCPDS	Joint Committee on Powder Diffraction Standards

Chapter one

Introduction

1- Introduction

1-1 General 1ntroduction

Recently, the fast-growing industries and population size lead to the formation of water pollution which causes the environment and human health problems (Ahmad et al., 2018). The wastes from industrial area such as textile dyes, pharmaceutical, dyeing, paper and pulp industries are the main sources of organic and inorganic compounds and a cause for water pollution . Particularly, organic dyes released from industries had severe health problems, toxic, indestructible, bio-recalcitrant, mutagenic, carcino-genic and have potential to fade resistant . Due to this reason, appropriate methods are needed to remove these organic pollutants before they are released to the environment Among the methods, photocatalysis is one of effective and efficient candidate technology used in wastewater treatment. The method is low cost, environmental benign and leads to complete min-eralization of organic pollutants from wastewater. Among the promised photocatalys, semiconductor based heterogeneous catalysts have been studied and reported as efficient and effectively treatments methods (Fardood et al., 2018).

1-2 Nanotechnology

The principles in "nano-technology" entered the language, physics professor Richard Feynman utilized the concepts in his presentation at a Caltech American Physical Society conference on December 29, 1959. The emergence of nanotechnology as a discipline of study was sparked by this talk. Feynman was told by Albert R. Hibbs that his micromachines may be applied to medical procedures. In a 1974 research, Professor Norio Taniguchi of Tokyo Science University introduced the term "nanotechnology." In the late 1970s and early 1980s, Eric Drexler stressed the promise of molecular nanotechnology. Scanning tunneling microscopy was developed in the year 19 Engines of Creation by Eric Drexler, the first book on nanotechnology, was released in 1986. (Adya ea tl., 2020) Atomic and molecular structures having at least one dimension in the nanoscale range and changin (1~100 nm) g composition, shape\morphology, size, or surface qualities are the focus of nanotechnology and nanoscience (Nasrollahzadeh et al., 2020 A nanomaterial, the International Organization for Standardization claims, is a substance with at least one exterior measurement at the nanoscale. In addition to their extremely small size, nanoparticles can also be categorized according to their form or chemical make-up. Depending on their chemical composition. (Rhazouani et al., 2021).

1-2-1 Applications of Nanotechnology

1- Treatment of water.

2- Food Additives (Niculescu et al., 2022).

3- Applications in Drugs and Medications.

4- Energy Application.

5- Agriculture Application.

6- Diagnostic Application of nanoparticle (Jadhav et al., 2021).

1-3 Classification of Nanomaterials

During the past decade, nanomaterials have been classified into different groups based on different criteria. The idea of the first classification of nanomaterials was introduced by Gleiter in 1995, and explained by Skorokhod in 2000 (Alkaç, et al., 2021) They are classified according to their dimensions, morphology, state and chemical composition, this classification is also based on their size, which ranges from 1 to 100 nanometers in at least one the dimension. Based on their overall dimensions and shape for this material, NMs (nano materials) can be divided into four classes (Saleh et al ,2020)

1-3-1 Zero-dimensional Nanomaterials

All three dimensions of these materials are nanoscale size (i.e., less than 100 nm). Graphene quantum dots, carbon quantum dots, fullerenes, inorganic quantum dots, magnetic nanoparticles, and noble metals are only a few examples (Wang et al., 2020).

1-3-2 One-dimensional Nanostructures

A scale smaller than 100nm, nanomaterials have two exterior dimensions. The micrometer (Lz > 100nm) is the last dimension. Nanotubes, nanofibers, and nanowires belong to this group (Erol et al., 2018).

1-3-3 Two-dimensional Nanostructures

Only one of the dimensions is located on the nanoscale while the other two are not. 2D includes thin films, nanosheets, and monolayer (crystalline or amorphous nanolayers). (Kolahalam, et al.2019)

1-3-4 Three-dimensional Nanostructures

These structures, such as nanocomposite, which consists of many phases on the premise that one of the solid phases is transitioning to the nanoscale, reveal nanoscale properties as a consequence of their internal nanoscale dimensions but have no exterior dimension in the nanoscale (Lee et al., 2018).

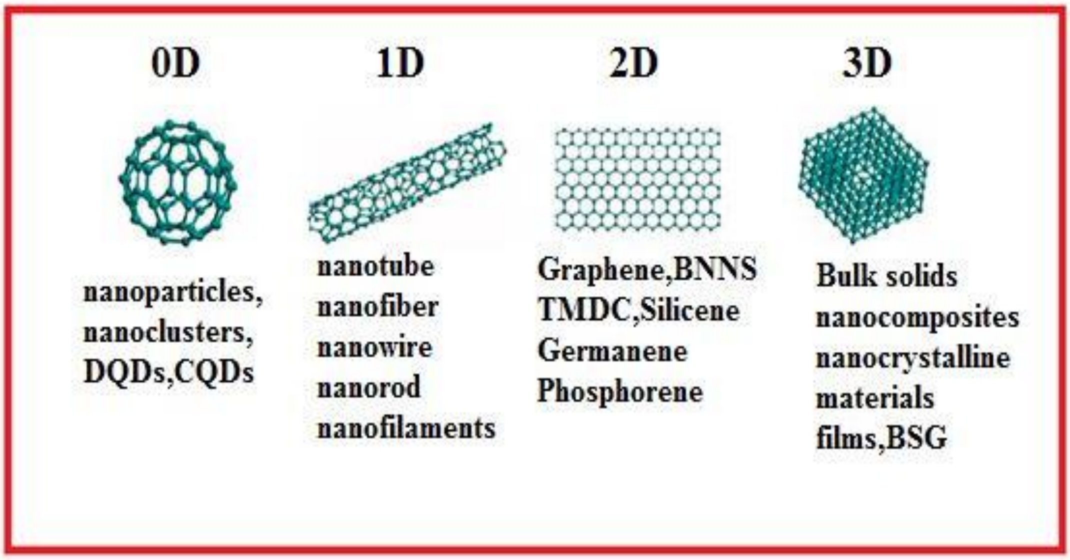

Fig. (1-1): Classification of nanomaterials depending on the dimensions (Barhoum et al., 2022).

1-4 Synthesizes of nanomaterales

Many methods are used for the preparation of metallic nanoparticles, which are divided into two categories: bottom up methods and top down approaches.

1- Top-down : the destructive technique is used in this procedure. Starting with a bigger molecule, it is divided into smaller units, which are subsequently turned into appropriate NPs. Grinding\milling (Khan et al., 2017).

2- Bottom-up: the approach to nanoparticle synthesis is based on the production of nanoparticles from smaller molecules, such as the combining of atoms, molecules, or tiny particles. In this approach, the nanoparticles' nanostructured building components are first created, then combined to make the final nanoparticle.

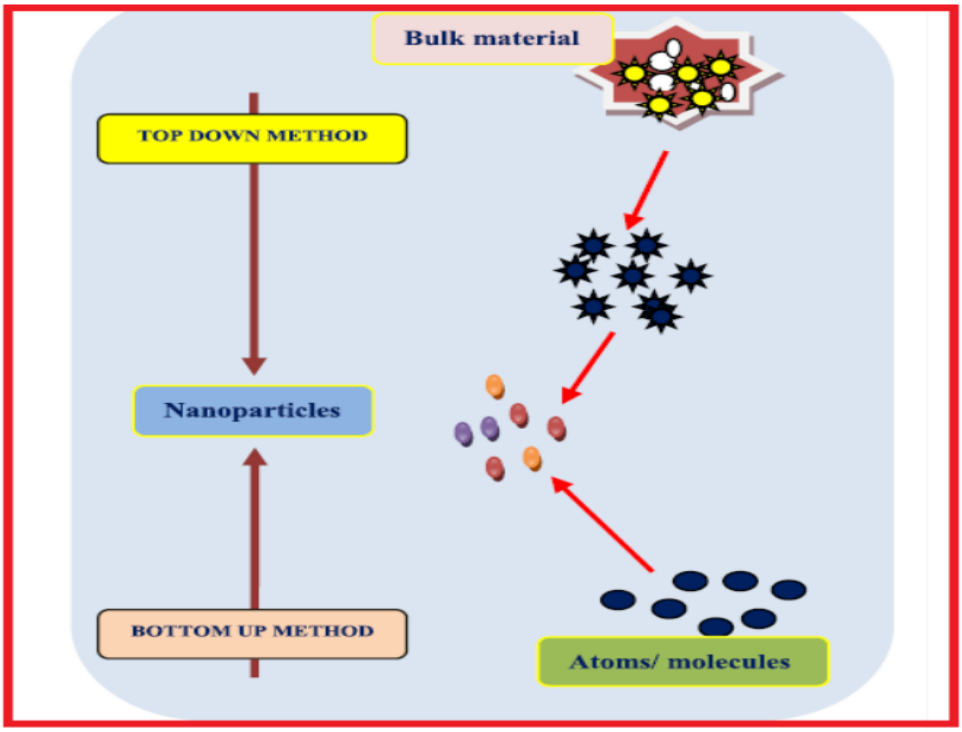

Fig. (1-2): The top-down and Bottom-up Methods for Nanoparticle Preparation. (Jamkhande et al., 2019)

Generally, nanomaterials can be synthesized by physical, chemical, biological or hybrid method of syntheses, In the physical method, one starts with bulk matter and then goes breaking down to smallerparticles till nano-scale size is achieved, a process called topdown

approach. Particular examples include laser ablation, where atoms are

removed from a solid through thermal or nonthermal process with intense

laser beam, physical vapor deposition, in which a material in the form of vapor particles are transferred from a source material(target) to the substrate and so on.

1-5 Hydrothermal Method

The hydrothermal method is a type of soft chemical synthesis method developed by simulating the formation process of some ores in nature. The hydrothermal technique involves heating and pressurizing an aqueous solution to produce a high temperature, high pressure reaction atmosphere. Then this reaction system is used as a reaction system in a unique confined reaction vessel (or the vapor pressure generated by itself). Under typical circumstances, a substance that is weakly soluble or insoluble is dissolved and recrystallized by the process (Yang, et al., 2019). Hydrothermal synthesis is the best technique for producing nanoparticles due to a number of characteristics. The resulting nanocrystals are empty defect-free, have a high specific surface area, little particle agglomeration, good crystallinity, high product purity, crystal symmetry, narrow particle size distribution, formation at a low temperature (200 °C), require little energy, and require inexpensive instrumentation. (Mamaghani, et al, 2018).

In the chemical synthesis method, nanomaterials are produced by combining substances in a wet chemistry and adjusting reaction parameters. In this method, atoms, molecules or ions in solution first form nucleation and then aggregates of those species that finally end up in particles of nano-size regime, a process called bottom-up approach.Nowadays, for synthesis convenience reasons, this is the most widely usedmethod of producing nanomaterials in industry So, there are various methods categorized under this approach including sol–gel, solvothermal,microwave irradiation, pyrolysis, chemical precipitation, microemulsion,thermal decomposition of precursors, etc. (Weldegebrieal et al., 2020)

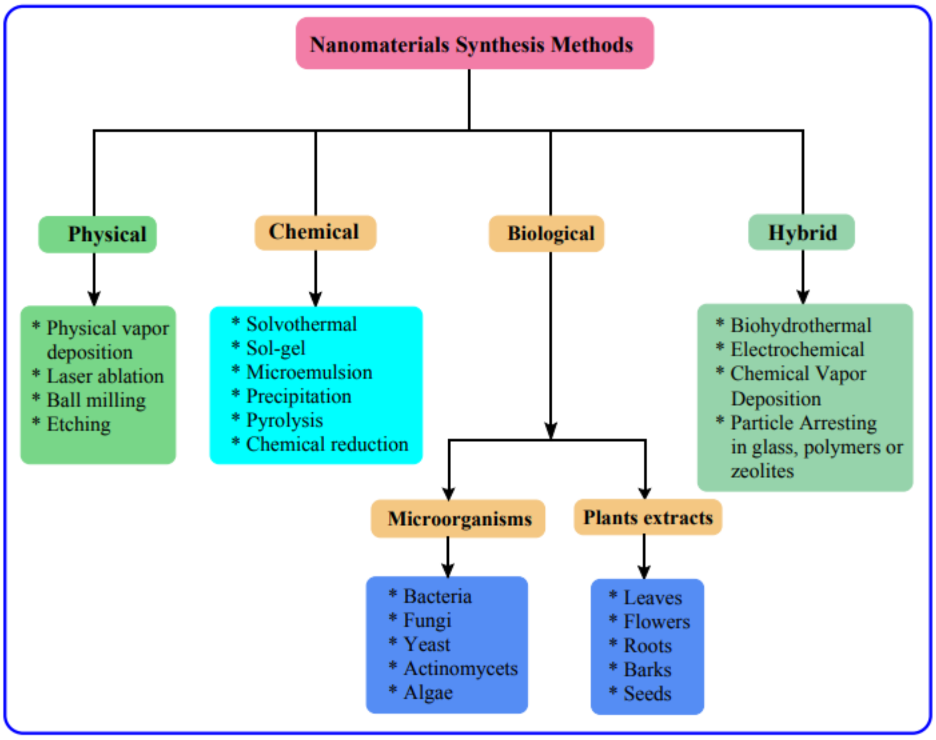

Fig. (1-3) Outline of general synthesis method of nanomaterials. (Weldegebrieal et al., 2020)

1-5-1 The Role of Water in the Hydrothermal Method

Water can be a chemical component in a hydrothermal reaction, as well as a solvent or an accelerator of puffing. By speeding the osmotic reaction and regulating the physical and chemical aspects of the process, inorganic compounds can be formed as a pressure transmission medium. In hydrothermal systems with high pressures and temperatures systems, the characteristics of water will result in the following modifications: : (1) The ionic product increases and the ionic product of water rapidly increases with the increase in pressure and temperature. Under high-temperature and high-pressure hydrothermal conditions, the hydrolysis reaction and ion reaction rates will naturally increase with water as the medium. According to the Arrhenius equation, dlnk/dt =

E/RT2 , the reaction rate constant has an exponential function with increasing temperature. Therefore, the main reason for the increase in the hydrothermal reaction is that the ionization constant of water increases as the reaction temperature and pressure increase. (2) The viscosity and surface tension of water decrease as the temperature increases. In hydrothermal systems, the viscosity of water decreases and the mobility of molecules and ions in solution greatly increases, such that crystals grow under hydrothermal conditions more rapidly than under other conditions. (3) The dielectric is often low and the dielectric constant generally decreases with increasing temperature and increases with increasing pressure. Under hydrothermal conditions, the reaction is mainly affected by temperature and the dielectric constant of water is significantly reduced. This decrease affects the ability and behavior of water acting as a solvent. (4) The density decreases, and properties, such as the viscosity, dielectric constant, and solubility of the material, increase with increasing density while the diffusion coefficient decreases with increasing density. (5) The vapor pressure increases and accelerates the reaction by increasing the chance of collision among molecules (Yang, et al., 2019).

1-6 ZnO nanopartical

Zinc oxide (ZnO) is a wide band gap (3.37 eV) semiconductor with a large exciton binding energy (60 mV) and one of the most widely used and studied functional oxides. Zinc oxide readily forms into noncentral symmetric wurtzite nanocrystal structures with self-polarized crystal surfaces. The thermodynamically stable crystallographic faces of ZnO include apolar-terminated (001) face and nonpolar low-symmetry (100) faces. The low- symmetry surfaces are more stable than the polar face, leading to faster growth along the polar surface. As a result, a variety of one-dimensional (1D) ZnO nano-structures including nanorods\nanowires, nanobelts, nanorings and other hierarchical nanostructures can be readily synthesized and these materials have been examined for applications in photovoltaic energyconversion, optics, optoelectronics, catalysis, piezoelectric systems, photocatalysts, chemicalsensors and solar cells. (suresh babu et al.,2013)

1-6-1 Crystal Structures of ZnO

ZnO is one of the most significant nanomaterials that has been widely studied for many decades, generally, ZnO crystallizes in three forms hexagonal Wurtzite, cubic zinc blende and cubic rock salt as in Figure (1-4). It is obtained only at optimum pressure and temperature. The crystal structure is composed of two interpenetrating hexagonal-close - pack (hcp) sublattices. (Mousavi, et al.,2022).

One sub-lattice consists of four O^{2-} and Zn^{2+} ions in one-unit cell forming a tetrahedron structure sp3 covalent bonding. The strongest polarity surfaces are due to the positively charged for 0001 - zinc polar surface and negatively charged for 0001 - oxygen polar surface. The two important features of the Wurtzite structure are the polar surfaces and noncentral symmetry. When a stress force is applied, the non-central symmetric structure will due to the separation of the central point of negative charges and that of positive changes leads to a temporary polarization (Corrado, et al,2019).

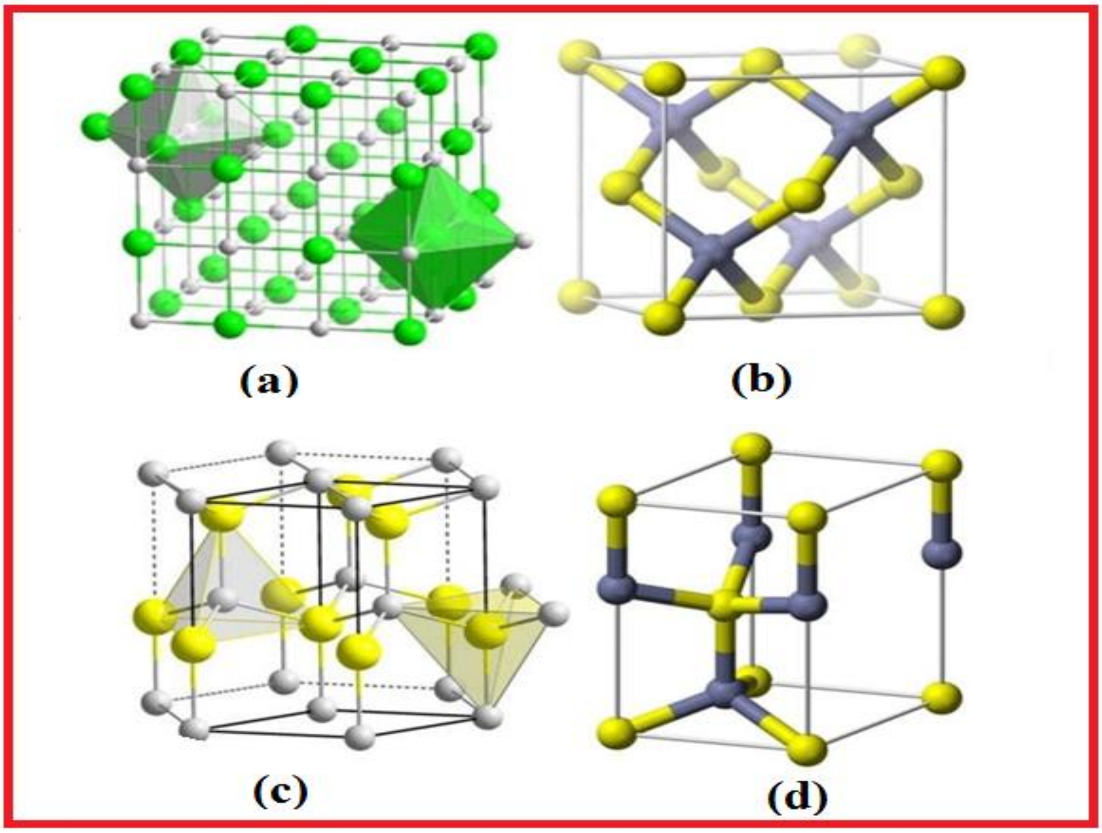

Fig. (1-4): ZnO crystal structures are shown as sticks and balls in the following order: (a) the rock-salt structure; (b) the cubic zinc blende unit; (c) the wurtzite structure; and (d) the wurtzite structure unit cell.

1-7 Chromium(III)Oxide

Chromic oxide nanoparticles (Cr_2O_3 NPs) are one of the notable inorganic NPs with outstanding features for several branches of modern science and technologies. Various fabrication approaches have been employed in the production of Cr_2O_3 NPs so as to meet its crucial potential. The ecological impacts and economic obstacles connected to most of the means of Cr_2O_3 NPs synthesis have contributed to the search for other alternative approaches with economic and environmental advantages. Surprisingly, the biological approaches to manufacturing using plant materials have been found suitable for the synthesis of Cr_2O_3 NPs dues to its myriad health, environmental, economic, and medicinal advantages. The important aspects of Cr_2O_3 NPs fabricated using plant broths and biomass augmented its application in antibacterial, antifungal, antioxidant, anticancer, antileshmanial, antiviral, and antidiabetic. In the area of electronics, chemistry and medicine, phytosynthesized Cr_2O_3 NPs have attracted tremendous usage in the fabrication of antibacterial, antifungal, antioxidant, anticancer, antileshmanial, antiviral, antidiabetic, photocatalytic agents as well as fabrication of microelectronic circuits, sensors, solar energy collectors and fuel cells. Notwithstanding, the enlisted advantages of biogenically produced Cr_2O_3 NPs, the challenges involved in the clarification of formation reaction still remain unsolved. This review presented the overview of the modern improvements in the synthesis, characterization methods, and applications of phytosynthesized Cr_2O_3 NPs in medicine, and pharmaceutical industries (Suresh et al, 2021) .

1-8 Advance Oxidation Process(AOPs)

AOPs are technologies that oxidize various organic pollutants in impure water to create clean water for human use, such as drinking and other household purposes. (Sharma et al., 2018). Antibiotic breakdown is aided by advanced oxidation processes (AOPs), which has piqued researchers' curiosity. Because of its low cost and high removal efficiency, the Fenton process has been widely employed for wastewater treatment. The so-called Advanced Oxidation Processes (AOPs) are a collection of technologies that are similar but not exactly the same and that rely mainly (but not exclusively) on the production of extremely reactive hydroxyl radicals. AOPs include electrochemical reactions and wet oxidation processes. Examples of photocatalysis, both heterogeneous and uniform, include Fenton and Fenton-like processes, ozonation, sonar, microwaves, and g-irradiation. (Dewil et al., 2017) (Khan et al., 2020). AOPs are used to successfully remove pollutants in plants that produce drinking water, in wastewater treatment systems to remove biorecalcitrant micro-pollutants, and in disinfection techniques (including photo-assisted ones). These reactions are based on the generation of potent reactive species (typically radicals) capable of attacking and mineralizing nearly all oxidizable compounds (Marco et al., 2021).

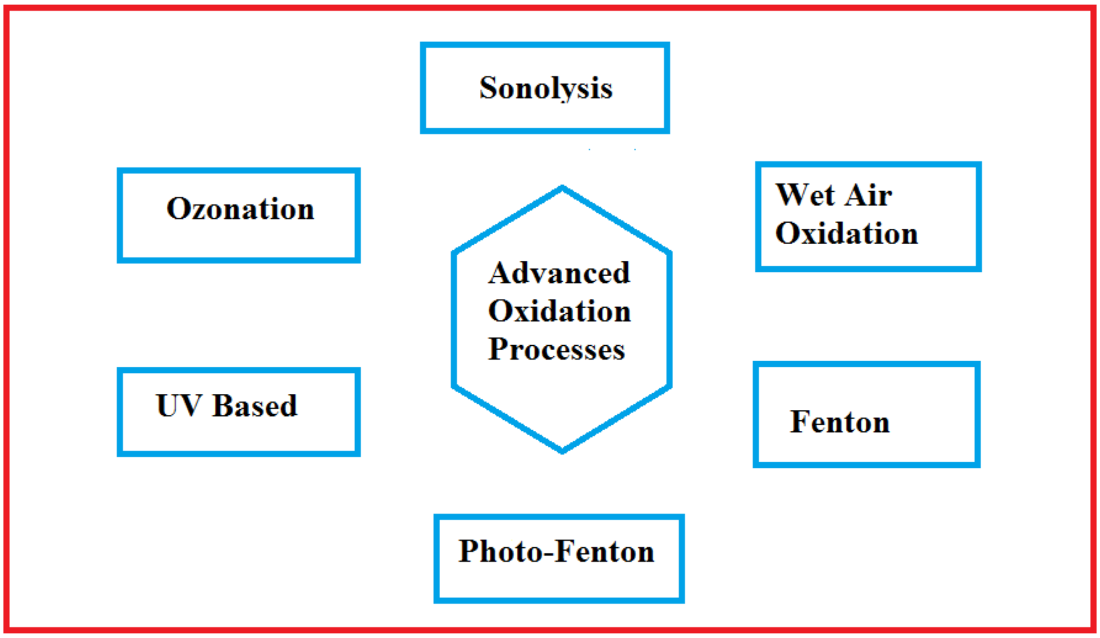

Fig. (1-5) : Classification of Advanced Oxidation.

1-9 Dyes

The textile industry is one of the biggest makers of liquid effluent contaminants because dyeing procedures require significant quantities of water. Additionally, the various manufacturing steps and kinds of synthetic dyes used during this change decide the various effluent characteristics in terms of pH, dissolved oxygen, organic and inorganic chemical content, and more. (Saratale et al., 2011). Textile dyes are one of the most common kinds of organic compounds that are causing water contamination. Azole dyes make up the majority of the dyes now on the market, with anthraquinone dyes following in second. UV and visible light irradiation have no effect on them. Additionally, they can be converted into carcinogenic aromatic amines in anaerobic or in vivo environments and are immune to aerobic breakdown (Madhavan et al., 2010). Azo dyes are the most common artificial hues used in daily living, especially when making fabrics. One or more azo bonds (-N=N-), which are found in combination with aromatic systems and auxochromes, can be used to identify azo pigments (–OH, $–SO_3$, and so on). Public health is at risk due to the discovery of cloth effluents that are poisonous, mutagenic, cancerous, and non-biodegradable. Adsorption, coagulation, photo-catalysis, ozonation, and biosorption are examples of physical, chemical, and biological processes that have historically been used to remove azo pigments from watery environments. These tried-and-true methods, though, have shown to be expensive time-consuming, and ineffectual. (Cai et al., 2016). Azo dye Compounds are used in a variety of industrial uses., including photodynamic therapy, photosensitivity, and biological activity due to their use in anti-inflammatory, antibacterial, and antifungal treatments (Karim et al., 2019).

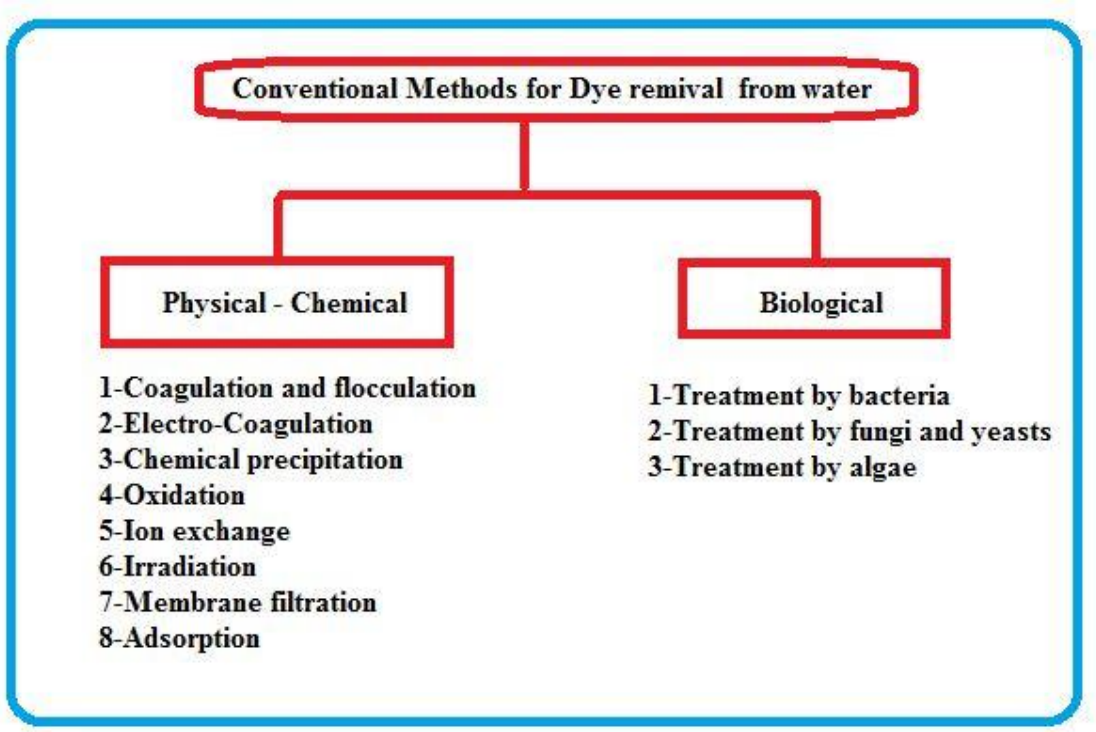

Fig. (1-6)：Treatment methods for the removal of dyes from wastewater effluent (Saratale et al., 2011).

1-10 Classification of dyes

There are just a few natural dyes available prior to the invention of synthetic colors. Since the annual global output of dyes has increased, the classification of dyes has become necessary. At several tens of millions of tonnes, they are thought to exist (Benkhaya et al., 2020).

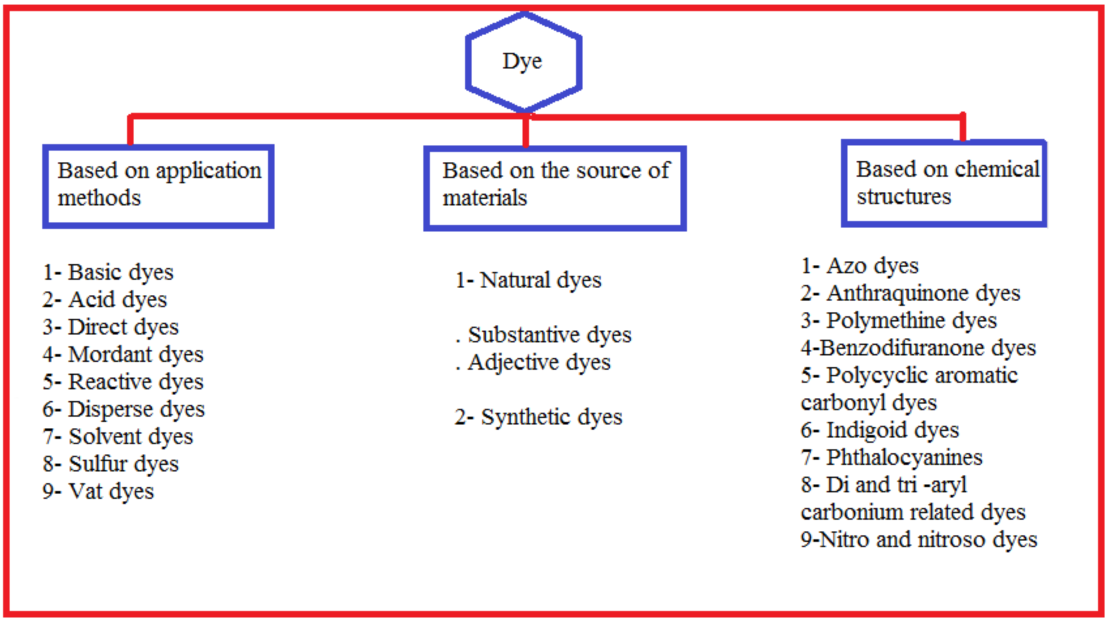

Fig. (1-7): Schematic diagram for classification of dyes according to their chemical structure and method of application (Benkhaya et al.,2020).

1-11 Fuchsin acid dye

Dyes are organic colorants that are typically composed of water-soluble materials and are progressively being used in a variety of global sectors. One of the pollutants discovered in industrial effluent is the dye carbol fuchsin (CF), which has the molecular formula $C_{20}H_{17}N_3Na_2O_9S_3$. CF is a combination of phenol and basic fuchsin (BF), a frequent crimson pigment used for biological staining as well as dying a variety of materials, including leather, paper, and cotton. Typically, cation-exchange screens are used to clean dye-contaminated water. (Abu-Zurayk et al., 2021)

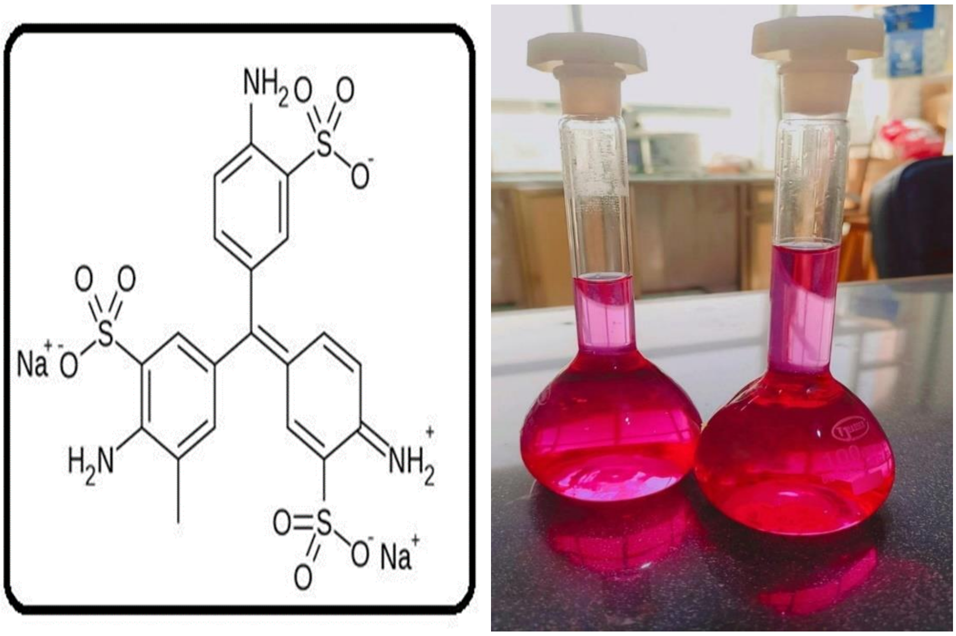

Figure (1-8): Chemical structure of Acid Fuchsin dye

1-12 Pinciples of Heterogeneous Photocatalysis

Heterogeneous reactions have risen in prominence among the various types of chemical reactions in recent years. Heterogeneous reactions, particularly in industrial fields, necessitate solid catalysts. Indeed, heterogeneous environments are used in 80 percent of commercial catalytic processes today. Among the many types of heterogeneous reactions, surface reactions on a solid have received considerable study. On the other hand, owing to technological limitations, heterogeneous processes in other systems have not been thoroughly studied from a macroscopic viewpoint. In liquid–liquid heterogeneous materials, for example, phase separation is difficult, and optical spectroscopic investigation is difficult due to the substantial light scattering generated by heterogeneity (Masuda et al., 2020)Heterogeneous photo catalytic techniques have been used in the last ten years to eliminate organic and inorganic contaminants from carbon dioxide and water using semiconductor oxides, metal oxides, and sun lamps.Zinc oxide is one of the most important semiconductors because it is a highly stable, inexpensive metal oxide that is both nontoxic and environmentally benign (Al-Gubury et al., 2018).

1-13 Literature Review

Sang, et al (2000) In this study ZnO/Cr_2O_3 catalyst (Zn: Cr=2: 1 in molar ratio) was prepared by a co-precipitation of the corresponding metal nitrates. The stability and the activity of Fe_2O_3/Cr_2O_3 and ZnO/Cr_2O_3 catalysts were examined for a reverse-watergas-shift reaction.

Michael, et al (2003) Reports that the Cr_2O_3\ZnO composite were prepeared using co-precipitating method. Many technique has been used to study thecharacterized by X-ray diffraction (XRD), N2-BET, and activity for methanol synthesis at 593 K. XRD and BET analyses.

Mancić, et al (2004) they reach to prepeared, spinel phase in Cr_2O_3\ZnO. XRD research was used to look into the development of the nanostructure in particles made either through solution-based (spray pyrolysis) or solid-state (mechanical activation) synthesis processes. The application of the computation based on atomistic techniques for the description of both defect and flawless spinel $ZnCr_2O_4$ crystal lattices allowed for the identification of specific structural flaws.

Kaiyuan, et al, (2012) was prepeared, Cr_2O_3\ZnO composite using the sol-gel technique, photocatalytic activity has been studied using methyl orange dye as model and mercury light of 300W .From the results, Cr_2O_3\ZnO composite show higher activity under the irradiation of a 300 W mercury lamp Comparing with pure ZnO or Cr_2O_3

Jyoti, et al (2015) represents nanomaterials were synthesized by hydrothermal method by varying the molar ratio of metals salts followed by calcination at 500 °C. ternary $Fe_2O_3/ZnFe_2O_4/$ ZnO nanocomposite has been prepeared, the crystalline phase, surface morphology and size of the prepared nanomaterials were characterized by XRD, FESEM & TEM analysis. FESEM and TEM images photocalaytic activity was studied using malachite green dye.

Mun Lam, et al (2018) successfully synthesized Cr_2O_3 particles anchored on the ZnO nanorods (Cr_2O_3/ZnO) by a hydrothermal deposition technique, the photocatalytic results showed that the phenol degradation by Cr_2O_3 /ZnO heterostructures was higher than those of pure ZnO and commercial TiO_2.

Nagabandi, et al (2019) They succeeded to prepeared ZnO-Cr_2O_3 nanocomposites by using co-precipitation method. The structural characterization was investigated using XRD, Gas sensing properties of the fabricated sensors were studied at room temperature and observed the superior sensing performance of ZnO-Cr_2O_3 sensor towards ammonia at room temperature.

AbdulKareem, et al (2021) prepared Cr_2O_3\ZnO nanofilm by pulsed laser deposition (PLD) technique at different concentration of ZnO. The surface topography was investigated and analyzed using an atomic force microscope (AFM), and optical gap values varying from 2.50 to 2.78 Electron Volt were noted. gas sensors properties for ZnO-doped Cr_2O_3 thin films were investigated in an reducing ammnia gas sensor

1-14 Aims of the present work

The main goal of this thesis is to find safe and economic methods for photocatalytic degradation of fuchin acid dye using UV irradiation and Cr_2O_3/ZnO nanocomposite .

1- Preparation of zinc oxide nanoparticles by hydrothermal method from zinc acetate dehydrate and oxalic acid.

2- Synthesis of Cr_2O_3/ZnO nanocomposite by hydrothermal method from zinc acetate dehydrate and oxalic acid and chromium oxide.

3- Characterization of prepared zinc oxide nanoparticles and Cr_2O_3/ZnO nanocomposite to determining various properties, by using XRD, FTIR, UV-vis spectroscopy, band gap , SEM and TAG.

4- Study of different operational parameters such as catalyst loading, initial dye concentration, pH and temperature on the rate of photo-degradation of the fuchin acid dye.

5- Study the kinetics of the photo-degradation of fuchisn acid dye in presence Cr_2O_3/ZnO nanocomposite photocatalyst and UV radiation.

6-Study the Thermodynamic parameters such as ΔH,ΔS,ΔG can be estimated according to Eyring equation and Activation energy was calculated using Arrhenius equation, of the photo-degradation of acid fuchsin dye in presence Cr_2O_3/ZnO nanocomposite photocatalyst and UV radiation.

7-Determine the average crystallite sizes by applying Scherer's´ equation.

8- Study the parameters that affect the degradation efficiency of fuchsin dye including the initial concentration of pollutants, masses of Cr_2O_3/ZnO nanocomposite, pH of solution, effect of presence of peroxides, effect of scavenger, and effect of temperature.

Chapter Two

Experimental Part

Methodologies

2.1. Chemical Materials

The chemicals were used as received without any further purification

Table (2-1): Chemicals used and respective suppliers

NO.	Name of substance	Chemical formula	Supplied company	Purity %
1	Chromium (III) Oxide	Cr_2O_3	Indian Production	98
2	Sulfuric acid	H_2SO_4	British Drug Houses (B.D.H)	98
3	Hydrogen Peroxide	H_2O_2	Indian Production	30
4	Fuchsin acid dye	$C_{20}H_{17}N_3Na_2O_9S_3$	Indian Production	98
5	Ethanol	C_2H_3OH	Merck Germany	98
6	Ascobic acid	$C_6H_8O_6$	CDH) Central Drag House	98
7	EDTA	$(CH_2N(CH_2CO_2H)$	CDH) Central Drag House	97
8	Sodium hydroxide	NaOH	CDH) Central Drag House	97
9	Hydrochloric acid	HCl	Sigma –Aldrich	35

10	Sodium azide	NaN_3	India Production	98
11	Zinc acetate di hydrate	$Zn(CH_3COO)_3.2H_2O$	Sigma-Aldrich	99.99
12	Oxalic acid	$C_2H_2O_4$	India Production	99.8

2.2. Instruments Analysis

Table (2-2): Instruments used in this study

No.	instrument	Company	Position of instrument
1	Furnace	Furnace Size - Tow Gallenkamp , South of Korea	Babylon University \ Collage of Science for women \Chemistry Department
2	Centrifuge	CL008 , JANETZI – T5, Belgium	Babylon University \ Collage of Science for women \Chemistry Department
3	Dried oven	LDO – 060e , Labphy , Korea	Babylon University \ Collage of Science for women \Chemistry Department
4	Fourier-Transform Infrared	SpactraIR-2, Instrument, USA	Babylon University \ Collage of Science for women \Chemistry Department

5	Hotplate Magnetic Stirrer	LMS-1003, HANNA instruments ,Lapphy England	Babylon University \ Collage of Science for women \Chemistry Department
6	pH meter	HI 83141 , Hanna, Romania	Babylon University \ Collage of Science for women \Chemistry Department
7	Scanning electron microscopy	SEM, Zeiss , Germany	Tehran University, IRAN
8	Sensitive electronic balance	3003- Denver instrument , Germany	Babylon University \ Collage of Science for women \Chemistry Department
9	Ultrasonic path	405 power sonic , Hwashin , korea	Babylon University \ Collage of Science for women \Chemistry Department
10	UV-visible spectrophotometer Single beam	UV mimi-1240 , shimadzu , Japan	Babylon University \ Collage of Science for women \Chemistry Department
11	X- Ray Diffractometer	XRD6000, Shimadzu, Japan	Ministry of Sciences and Technology, IRAQ
12	Thermo gravimetric analysis (TGA)	DTG-60 , Shimadzu, Japan	Babylon University \ Collage of Science for women \Chemistry Department

13	Hydrothermal System	Binder , Germany	Babylon University \ Collage of Science for women \Chemistry Department
14	UV.Visible diffuse reflact	Aa	Babylon University \ Collage of Science for women \Chemistry Department
15	Oven	Memmert,Germany	Babylon University \ Collage of Science for women \Chemistry Department

2- 3 Methodologies

2-3-1 Preparation of Zinc oxide nanopartical

The synthesis of zinc oxide NPs were made utilising a hydrothermal method that included the use of zinc acetate dehydrate and oxilic acid as precursors, as described in the literature (Worasawat et al, 201). For this situation, (5g)of zinc acetate dehydrate has been disolved in (50mL) distilled water with constant stirring for 15 minutes at 298k. Meanwhile a(3g) of oxilic acid di hydrate has been disolved in (50mL) distilled water under stirring for same duration. After the zinc acetate dehydrate and oxilic acid was completely dissolved, the mixture was prepared by slowly adding oxilic acid solution drop by drop to zinc acetate dehydrate solution , while magnetic stirring was kept at high speed. The process was permitted to continue for 1 hour. This solution mixture was transferred into Teflon lined sealed stainless-steel autoclaves and kept in hydrothermal oven at a temperature of 160 °C for 24 h. Then the solution allowed to cool naturally to room temperature. The resultant solution was filtered, the white precipitate of ZnO NPs washed with distilled water, ethanol and kept for drying .The final product was calcined at 600°C for 2 hr.

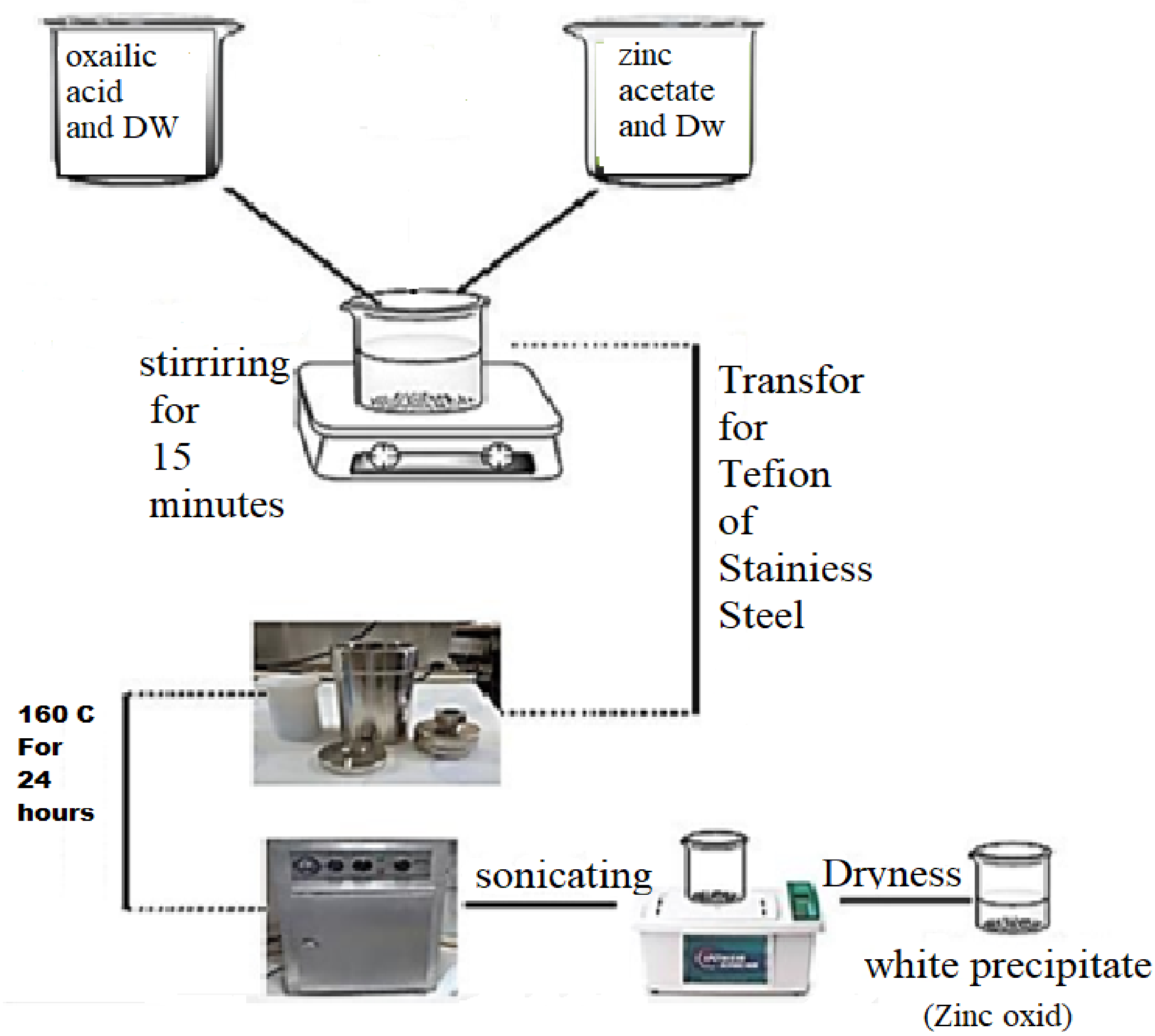

Fig. (2-1): Prepration zinc oxid nanopartical.

2-4 Synthesis of Cr_2O_3\ZnO nanocomposite

Nanoscale Cr_2O_3\ZnO composites were successfully synthesized via hydrothermal route. (5g) of zinc acetate dehydrate has been disolved in (50mL) distilled water with constant stirring for 15 minutes at 298k. Meanwhile a(3g) of oxilic acid has been disolved in (50mL) distilled water under stirring for same duration. After the zinc acetate dehydrate and oxilic acid was completely dissolved, the mixture was prepared by slowly adding oxilic acid solution drop by drop to zinc acetate dehydrate solution , while magnetic stirring was kept at high speed. 1g of Cr_2O_3 were dissolved in in 70ml distilled water and added to the mixture of zinc oxide nanoparticle with continuous stirring until get homogeneous solution. The solution was placed in a Teflon-lined autoclave and aged at 160 °C. The The reaction powder obtained was filtered and washed twice with water, ethanol and acetone, then dried at room temperature overnight. Finally, the mixture powders were calcined at 600°C in the air for 2 h to obtain Cr_2O_3/ZnO composites(Qixuan et al,2017).

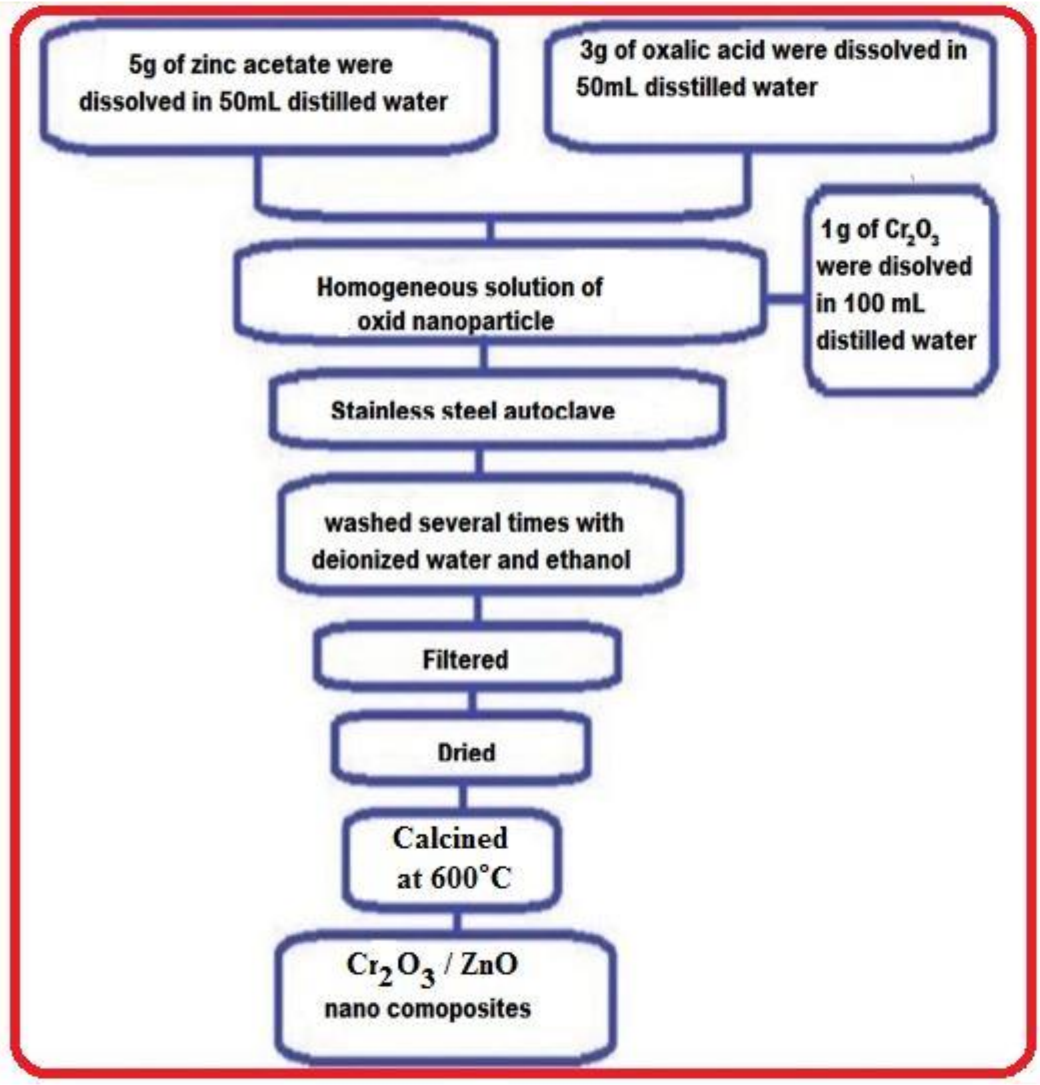

scheme (2-2) Synthesis of Cr_2O_3\ZnO nanocomposites Using hydrothermal process.

2- 4-1 X-ray Diffraction Analysis

The crystalline quality of the ZnO, Cr_2O_3, and Cr_2O_3\ZnO nanocomposite, particle size, phase composition, and average spacing layers\rows of at-oms were examined using an X-ray diffractometer. A Shimadzu XRD6000 was used to conduct the study. At 40kV, 30mA, and 45 Cu K radiation (= 1.54056 A°), a rate of 5 degrees per minute, and a range of 2 degrees, the measuring conditions were set (3- 60). The lattice planes of a crystal are divided by d. Braggs' law were used to calculate the inter-plane spacing (d).describes the length of the mirrored X-wave beam (λ**),**), the distance (d) between atomic planes as in equation

$n\lambda = 2d \sin\theta$ **............ (2-1)**

n : is the diffraction order (n =1 is first order, n=2 is second order,n=3 is third order.

λ :is the wavelength of the X-ray that incident on the crystal surface.
d :is the distance between the atomic layers.

Ɵ : is the angle with which the X-ray incident on the crystal surface

Using Debye–Scherrer's equation, and the size of the synthesized Cr_2O_3\ZnO nanocomposite crystallite: was calculated using the strong peak's full width at half maximum (FWHM):

$$\mathbf{D = \frac{k\lambda}{\beta \cos\Theta}} \quad \textbf{......(2-2)}$$

D: The average crystallite size, while k is the Scherer's constant related to crystal shape, normally taken as 0.94 for homogeneous shape, whereas the value for heterogeneous shape is 0.89. =0.154 nm is both the (Cuk) X-ray wavelength and, **β** represent the full width at half maximum (FWHM) of the difraction peak in radians. θ is the Bragg difraction angle at which FWHM measure, λ: is X-ray radiation's wavelength.

2.4.2 Scanning Electron Microscope (SEM):

The SEM is an instrument that uses electrons to an SEM machine named ZESS EVO-50 was used for the examination. A little amount of the sample was applied to the grid, any surplus material was removed using blotting paper, and the sample was dried on the SEM grid for five minutes under a mercury lamp to generate thin films on a carbon-coated tape. The structure of the reaction products formed was determined by SEM analysis. (Mishra et al., 2015).

2.4.3 Fourier Transform Infrared Spectroscopy (FTIR):

The fuctinal groups on ZnO, Cr_2O_3 and Cr_2O_3\Zno was determined using a Jasco FTIR-460 plus spectrophotometer as well as FT-IR, or Fourier Transform Infrared Spectroscopy, in the wave number range of (4000-400 cm-1). KBr wafers are wafers constructed of KBr (Kumar et al., 2022).

2-4-4 Thermo Gravimetric Analysis (TGA)

Thermo Gravimetric Analysis (TGA) Analysis is a destructive analytical technique that analyzes the contents ofa sample using high-temperature pyrolysis. Carbon-based materials are frequently heated to (30-1000˚C) in an inert or oxidizing environment. This approach measures the change in mass of a sample(percent) as a function of time for a specific temperature

2-4-5 UV-Visble measurements

The band gap energy (Eg) of the synthesized Cr_2O_3\ZnO nanocomposite was determined by measuring the reflection spectrum (reflectance as a function of wavelength) using UV–vis diffuse reflectance spectra (UV–vis DRS). Kubelka-Munk method which is used to determine the Eg is based on the following equation

$$F(R) = \frac{(1-R)^2}{2R} \quad \text{.........} (2-3)$$

Where:
R: is reflectance; F(R) is proportional to the excitation coefficient.
By plotting $(F(R)h\nu)^2$ versus Energy, E (eV), Eg of nanocomposite can be determined. Where n=2 for an indirect allowed transition.
Energy can be calculated using equation below:

$$E_g = \frac{1240}{\lambda} \quad \text{............} (2-4)$$

By extrapolate from the band ege to get band gap in eV (Makula et al 2018).

2.5. Photocatalytic Reactor system

Fig (2-3) demonstrates that all experiments were conducted using the photocatalytic degradation system.

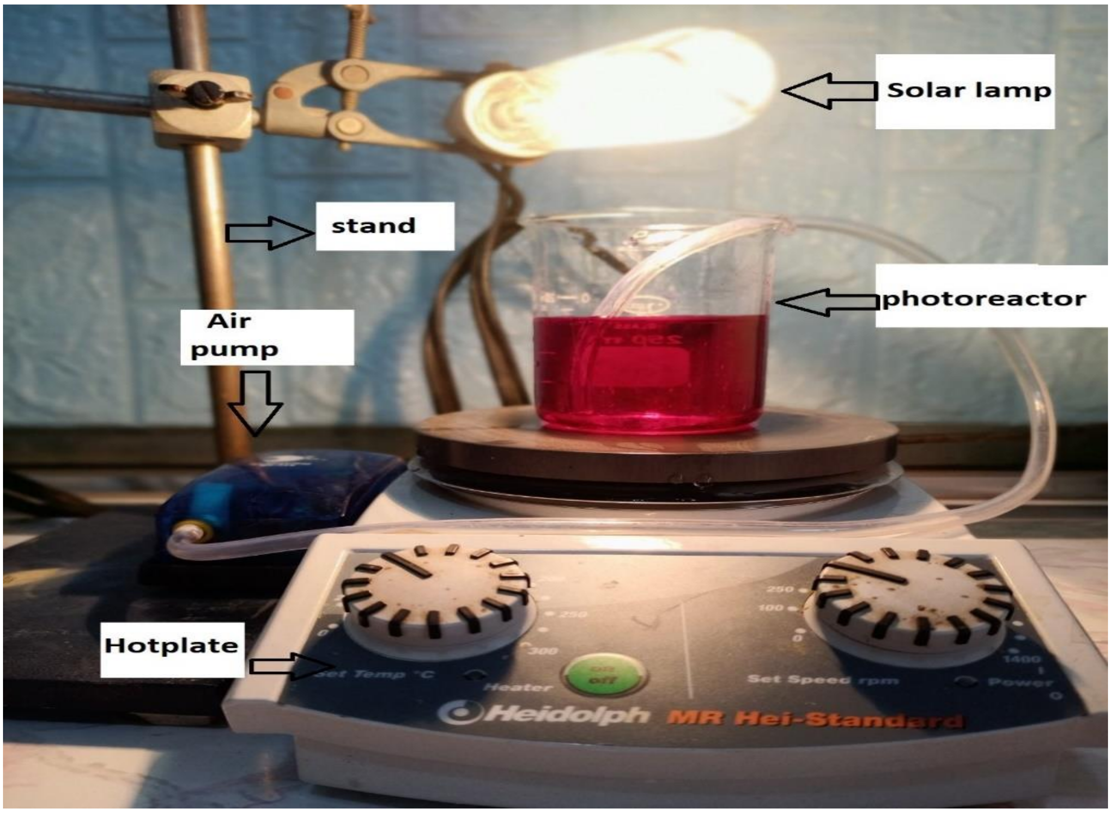

Fig. (2-3): Optical photo for main parts of the Photocatalytic degradation system.

2– 5–1 Measurements of photocatalytic activity

The photocatalytic degradation experiment was carried out using photocatalytic reactor system, which included all of the major components illustrated in Figure. (2-3). All photocatalytic measurements were performed using Fuchsin acid dye solution contained in a photo re-actor. A 20 mL from a 100 mg/L Fuchsin acid dye stock solution was di-luted to a volume of 100 mL using distilled water for a Fuchsin acid dye concentration of 20 mg/L. The quantity of Cr_2O_3\ZnO composites was kept the same throughout the experiment, using 0.13g/100mL catalyst for each degradation. The catalyst and Fuchsin acid dye solution were allowed to stir in the dark for 30 minutes in order to allow for adsorption of the Fuch-sin acid dye onto the surface of the Cr_2O_3\ZnO composites. The photo reactor was then irradiated by a mercury lamp with 125 W while stirring. Suspensions solution were sampled at regular intervals, 2-3 mL of the reaction mixture was withdrawn every 10 min, up to 60 min and centrifuged for 10 min. After the centrifuge, the absorbance at the maximum wavelength of Fuchsin acid dye (520 nm) was measured with UV-visible spectrophotometer.

2-6 Photocatalytic Experiments

The degradation of the dyes was performed by using fuchsin acid dye in precense Cr_2O_3\ZnO nanocomposites as the photocatalyst. This technique seems to be effective since complete degradation is achieved within 60 min under the experimental conditions. The photocatalytic efficiency (PDE) was evaluated using Equation as follow:

$$\text{PDE}\ \% = \frac{(A_0 - A_t)}{A_0} \times 100 \quad \text{..........} \ (2-5)$$

Where (A_0 and A_t) are the initial and remaining absorption at given time (t) respectively.

2-7 Applications of Prepared Nanomaterials

2-7-1. The Effect of Cr_2O_3\ZnO nanocomposites masses on the photocatalytic degradation of fuchsin acid dye

To measure the optimal mass of the Cr_2O_3\ZnO nanocomposites several sets of experiments were carried out using (0.03, 0.06, 0.013 ,0.16, and 0.2 g\100mL) of catalyst nanopowder introduced into a dye solution of 20 ppm in 100mL at 298k.

2-7-2. The Effect of the Initial Concentration dye on photocatalytic degradation process using constant mass of coupled of Cr_2O_3\ZnO nanocomposites.

Various studies were carried out with varying initial substrate concentrations of fuchsin acid dye (10, 20, 30, 40, and 70) mg\L with constant mass of (0.13 g\100mL) of Cr_2O_3\ZnO nanocomposites, (pH=9), temperature (298k).

2-7-3 The Effect of pH on the photocatalytic degradation process using Cr_2O_3\ZnO nanocomposites

The pH value of dye has a significant influence on the percentage of degradation of dye. The effect of initial pH value of solution was examined by varying pH of methyl orange solution (3, 5, 9, and 10) respectively .

2-7-4. The Effect of the H_2O_2 on the photocatalytic degradation of fuchsin acid dye

A series of experiment were carried out using (1,2,3,4 % (v\v)) to study the influence of H_2O_2 on photocatalytic dye

2-7-5. The Effect of the reactive oxidative species on the photocatalytic degradation of fuchsin acid dye

Several scavengers has been used to investigated the effect of reactive oxidative species (ROSs) such as $^{\bullet}OH$, $^{\bullet -}$ **O_2** and $1O_2$ on photocatalytic degradation of fuchsin acid dye.

2-7-6. Effect of temperature on the photocatalytic degradation process using Cr_2O_3\ZnO nanocomposites

The effect of temperature on photocatalytic degradation of fuchsin acid dye was investgated using different temperature (288, 298, 303, 308) K.

2-8 Measurement of the reaction rate constant

The typical Langmuir-Hinshelwood (L-H) model is used to study the kinetics of dye photodegradation over as-synthesised materials (Krishnakumar et al., 2011). Eq (2-6) which is expressed as

$$R = \frac{dc}{dt} = \frac{k_f K_a C}{(1+k_a C)} \qquad (2\text{-}6)$$

Where:

R: Rate of reaction, k_f: Rate constant (min^{-1}),

K_a: Langmuir adsorption constant,

C: Concentration (mg\L),

t: Time (min)

The Langmuir–Hinshelwood equation can be modified as:

$$\frac{1}{R} = \frac{1}{(k_f K_a C)} + \frac{1}{k_f} \qquad (2\text{-}7)$$

2-9 Thermodynamic Parameters:

2-9-1 Determination the activation energy:

According to the Arrhenius equation, the activation energy (Ea) is:

$$K = A\,e^{-Ea/RT} \qquad (2\text{-}8)$$

$$\ln K = \ln A - \frac{Ea}{RT} \qquad (2\text{-}9)$$

The equation establishes a link between reaction rate and temperature. K: The rate constant.

A: The frequency factor.

Ea : The reaction's Activation Energy. R:The gas constant

(8.314 J mol^{-1} K^{-1}), and T :The absolute temperature (Mohsin et al., 2013) (Kzar et al., 2019).

2-9-2 Determination enthalpy of activation and entropy of activation

From the plot of the Erying equation, the values of ΔH and ΔS can be computed as following

$$\ln\left(\frac{k}{T}\right) = -\frac{\Delta H}{R}\cdot\frac{1}{T} + \ln\left(\frac{K_B}{h} + \frac{\Delta S}{R}\right) \qquad (2\text{-}10)$$

where, K_B = Boltzmann’s constant [1.381×10^{-23} J\K].

T = absolute temperature in Kelvin (K).

h = Plank constant [6.626×10^{-34} J·s].

k : the rate constant.

ΔH and ΔS the enthalpy and entropy of activation respectively.

2-9-3 Determination Free energy of activation

The Gibbs' free energy ΔG may have computed using the following formula

$$\Delta G = \Delta H - T\Delta S \qquad (2\text{-}11)$$

ΔG :Change in Gibbs free energy.

ΔH : Change in Enthalpy.

ΔS : Change in Entropy.

T: absolute temperature in Kelvin (K).

2-10 Kinetic study of photodegradation:

Different experiments were conducted at the optimum condition, to check the suitability of the model for photocatalytic degradation of Cr_2O_3\ZnO nanocomposite. Tested both pseudo-first order reaction and pseudo-second-order reaction. The integrated forms of the pseudo-first order and pseudo-second-order models are according to Eq. (2-12) and Eq. (2-13), respectively

$$\ln \frac{A_0}{A_t} = k_1 t \qquad (2\text{-}12) \qquad \textbf{First order}$$

$$\frac{1}{A_t} = \frac{1}{A_0} + k_2 t \qquad (2\text{-}13) \qquad \textbf{Second order}$$

where $\mathbf{A_0}$ is the initial Absorbance.

$\mathbf{A_t}$: The Absorbance after time **t** .

Chapter Three

Results and Discussion

3- Results and Discussion

3-1 Characterization Cr_2O_3\ZnO nanocomposite

3-1-1 X-Ray Diffraction analysis for ZnO nanoparticles

The XRD pattern of pure zinc oxide nanoparticle were depicted in Table (3-1) and Figure. (3-1),exhibited the typical peaks. The peaks were observed at 2θ = 31.837˚, 34.502˚, 36.334˚, 47.650˚, 56.726˚, 63.012˚, 68.114˚, 69.254˚ and 89.860˚, which are corresponding to the crystallographic planes (100, 002, 101, 102, 110, 103, 112 and 201) respectively. zinc oxide could be indexed to the hexagonal (JCPDS 38–1479),The average crystallite sizes of synthesized ZnO nanoparticles were calculated applying Scherrers equation(42.76nm).

Table (3-1): Average crystal size(nm) of ZnO nanoparticles, 2 Theta \deg, FWHM \deg and I\\I_0.

Compound	2 Theta /deg	FWHM /deg	I/I_0	Interplanar distance (d)	Average Particle Size/nm
Zinc oxide	36.4073 31.9228 34.5797	0.20320 0.20540 0.18240	100 59 47	2.46579 2.80120 2.59181	42.76

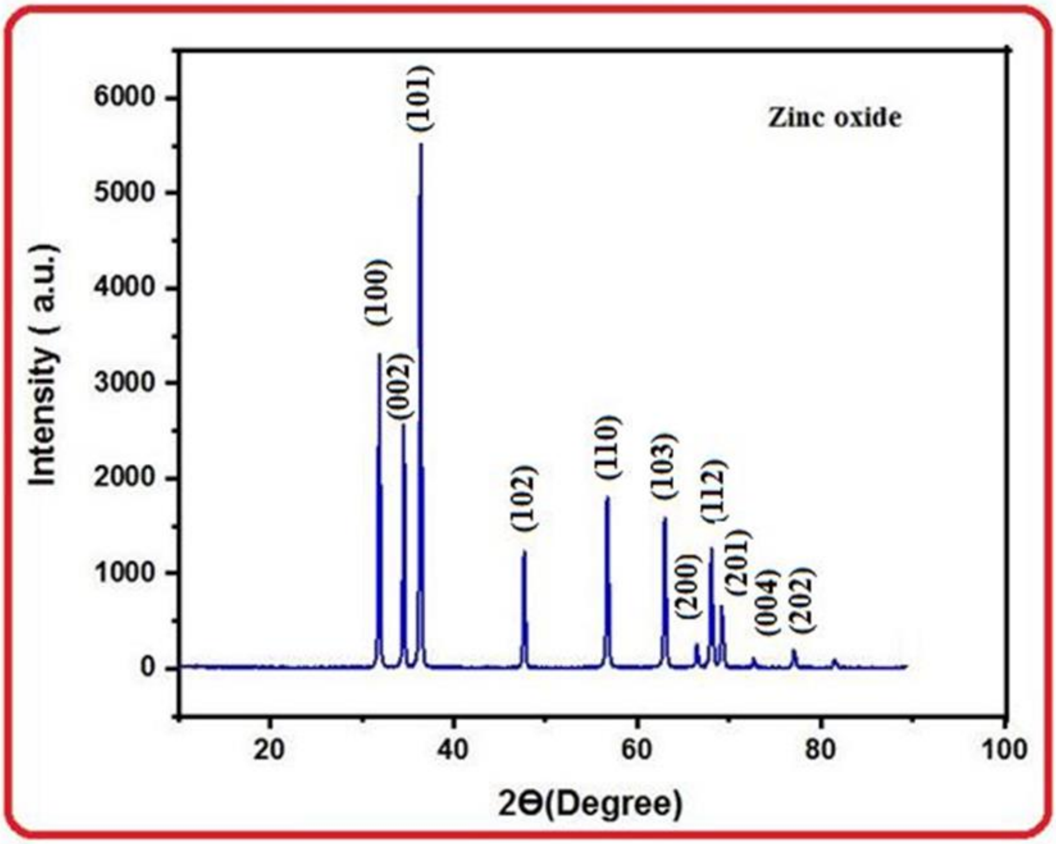

Fig. (3-1): XRD patterns of ZnO nanoparticles.

3-1-2 X-Ray Diffraction analysis for Chromium(III)Oxide

The XRD pattern of pure zinc oxide nanoparticle were depicted in Table (3-1) and Figure. (3-1),exhibited the typical peaks. The peaks were observed at 2θ = [21.3826 ˚,26.0844 ˚,31.2530 ˚, 38.0790 ˚,40.0649 ˚, 46.2634 ˚,49.5944 ˚, 54.2889 ˚, 69.3505 ˚, and 86.2419 ˚ respectively], which are corresponding to the crystallographic planes [220, 012, 104, 110, 006, 202, 924, 116, 300, and 134] respectively.The Cr_2O_3 is crystallized in rhombohedral structure . All the observed planes are excellent in accordance with the standard JCPDS card No. 96-900-8085. The average crystallite sizes of Chromium(III)Oxide nanoparticles were calculated applying Scherrers´ equation(23.1841nm).(Mohamed et al., 2021). As shown in Table (3-2) and Figure. (3-2).

Table(3-2):Average crystal size(nm) of Cr_2O_3 nanocomposite , 2 Theta \deg, FWHM \deg and $I\backslash I_0$.

Compound	2 Theta /deg	FWHM /deg	I/I_0	Interplanar distance (d)	Average Particle Size/nm
Chromium (III)oxide	21.3826 26.0844 26.4655	0.27770 0.28030 0.29160	100 79 56	4.15217 3.413441 3.36512	23.1841

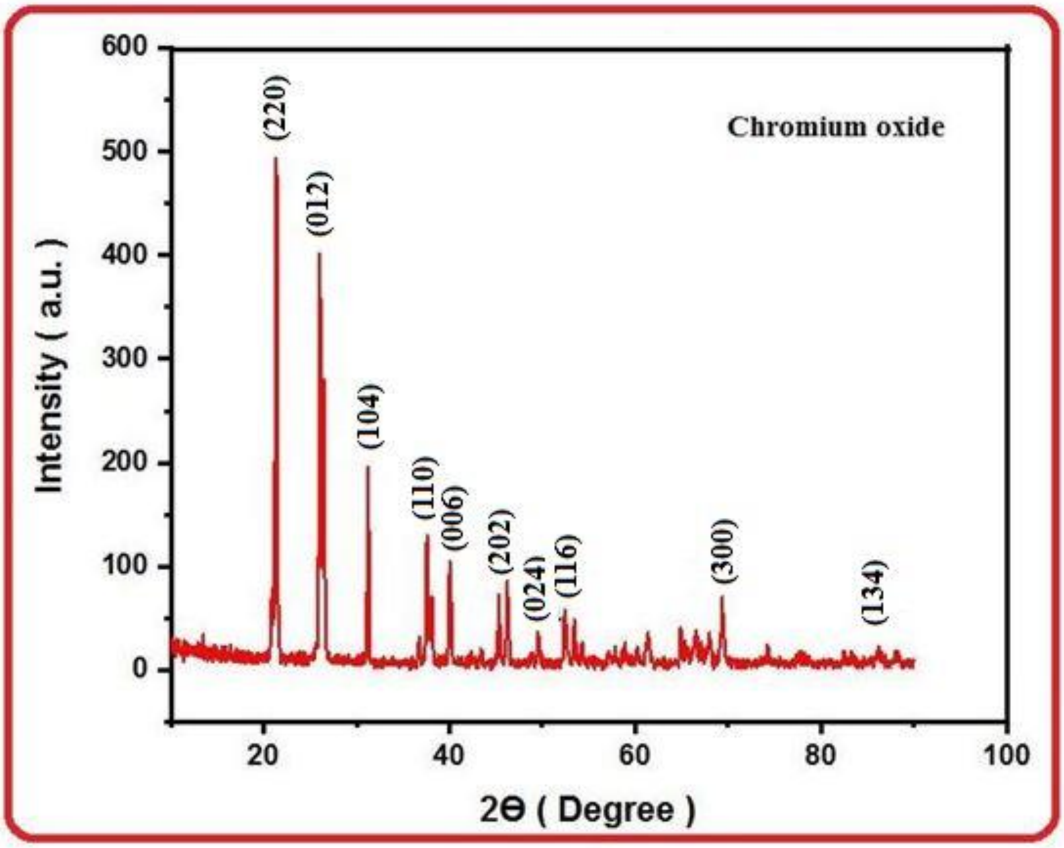

Fig. (3-2): XRD patterns of Chromium(III)Oxide

3-1-3 X-Ray Diffraction analysis for Cr_2O_3\ZnO nanocomposite.

Cr_2O_3/ZnO nanocomposite with characteristic peaks at 2Θ = (30.3156 °, 31.7662 ° ,35.7165 °,36.3367 °,43.4067 °,53.8741 °, 57.4143 °,63.0672 °,71.5208 °, and 74.6533 °) which are corresponding to the crystallographic planes [(*100 ZnO), (#104 Cr_2O_3), (*002 ZnO), (#110

Cr_2O_3) (#202 Cr_2O_3), (#116 Cr_2O_3), (*110 ZnO), (#214 Cr_2O_3), (*004 ZnO), and (*202 ZnO)] respectively.The highest-intensity peaks in the X-ray difraction pattern appeared at 2θ=35.7165, 63.0672,and 57.4143 were used to estimate the average crystallite size (D) of Cr_2O_3/ZnO nanocomposite using Debye–Scherrer's equation().The average crystallite size (D), maybe smaller or equal to(12.74 nm) (Mohamed et al., 2021) (Mahdi et al 2020). As clear in Table (3-3) and Figure. (3-3).

Table(3-3): Average crystal size(nm) of Cr_2O_3\ZnO nanocomposite 2 Theta \deg, FWHM \deg and I\\I_0.

Compound	2 Theta /deg	FWHM/deg	I/I_0	Interplanar distance (d)	Average Particle Size/nm
Cr_2O_3/ZnO nanocomposite	35.7165 63.0672 57.4143	0.63570 0.76780 0.61170	100 46 42	2.51188 1.47285 1.60368	12.74

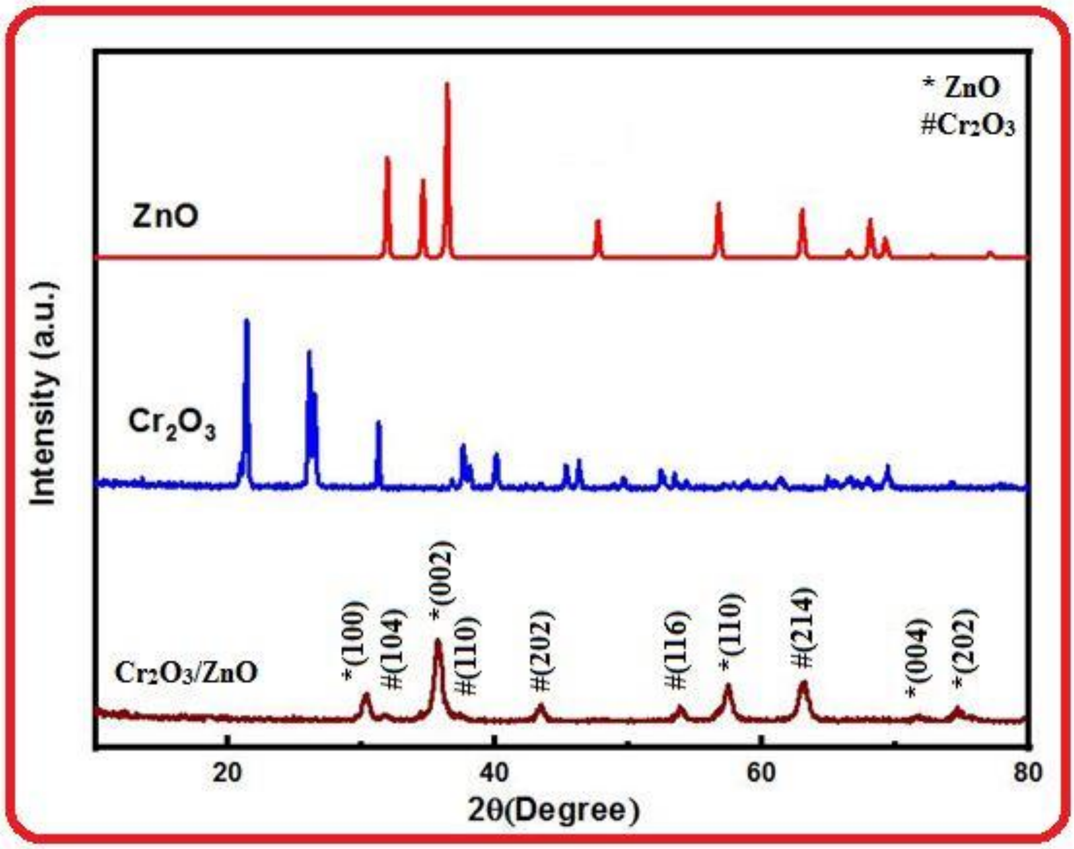

Fig. (3-3): XRD patterns of ZnO,Cr_2O_3,Cr_2O_3\ZnO nanocomposite.

3-1-4-1- FTIR Spectroscopy Synthesized ZnO NPS:

.FTIR spectra of synthesized zinc oxide consists of the peaksat(444.02,498.75,546.84,607.37,825.45,88018,1029.43,1111.52,1172.86,1376.88,1430.76,2370.23,2921.64,3350 cm^{-1}) .As shown in Figure. (3-4) The FTIR band characteristics assigned at 3348 cm^1 corresponds to the OH stretching of modes of water molecules. Stretching vibration modes of Zn-O is located at around 420 cm^{-1} characteristic peaks as reported in literature. Moreover, the band around and 623 cm^{-1} may be also attributed to the 621 cm^{-1} binding mode. Hence, it can be conclude that the Zn-O bond were formed successfully which are also the indicators for metals and oxygen bond formations in the prepeared zinc oxide nanoparticles. The band located at 2989 cm^{-1} represent (CO_2) groups. The band located

(C-OH) at 1041 cm^{-1}, band located (C-C) at 621 cm^{-1} (Shashanka et al., 2021) (Resmi et al., 2021).

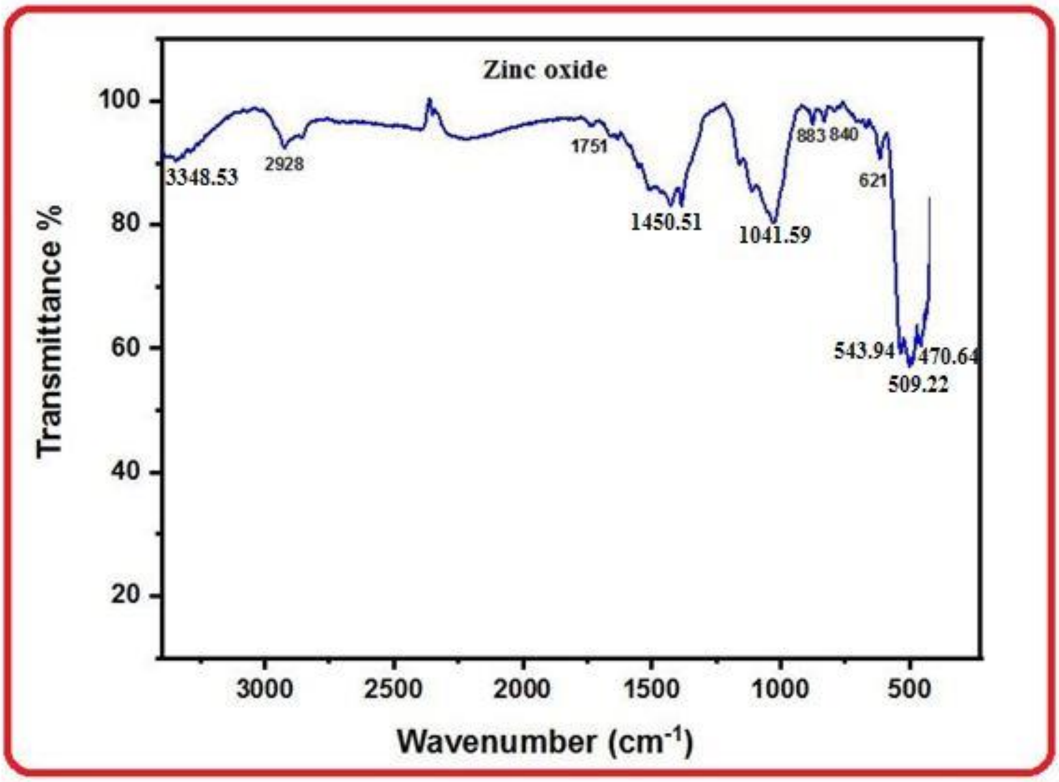

Fig. (3-4): FTIR spectra of synthesized Zinc Oxide NPS .

3-1-4-2- FTIR of Chromium oxide NPs:

FTIR spectroscopy of chromium oxide nanoparticles was performed using (Perkin Elmer model 1650) over the range of 400–4000 cm^{-1}. FTIR spectra of chromium oxide nanoparticles consists of the peaks at(459,754.19, 964.44, 1622.12, 2372.52, and 3329.24 cm^{-1}) .As shown in Figure. (3-5),the typical peaks in the FTIR spectra of chromium oxide nanoparticles weak absorption at 459 cm^{-1} of (Cr-O) single bond in bending mode, 754.19 cm^{-1} bending mode of (Cr-O),964.44 cm^{-1} strong vibration of (Cr-O),1622.12 cm^{-1} of (CO_2),2372.52 cm^{-1} of (C-H) vibration, and 3329.24 cm^{-1} of (OH) group. (Zhenzhao et al., 2016)

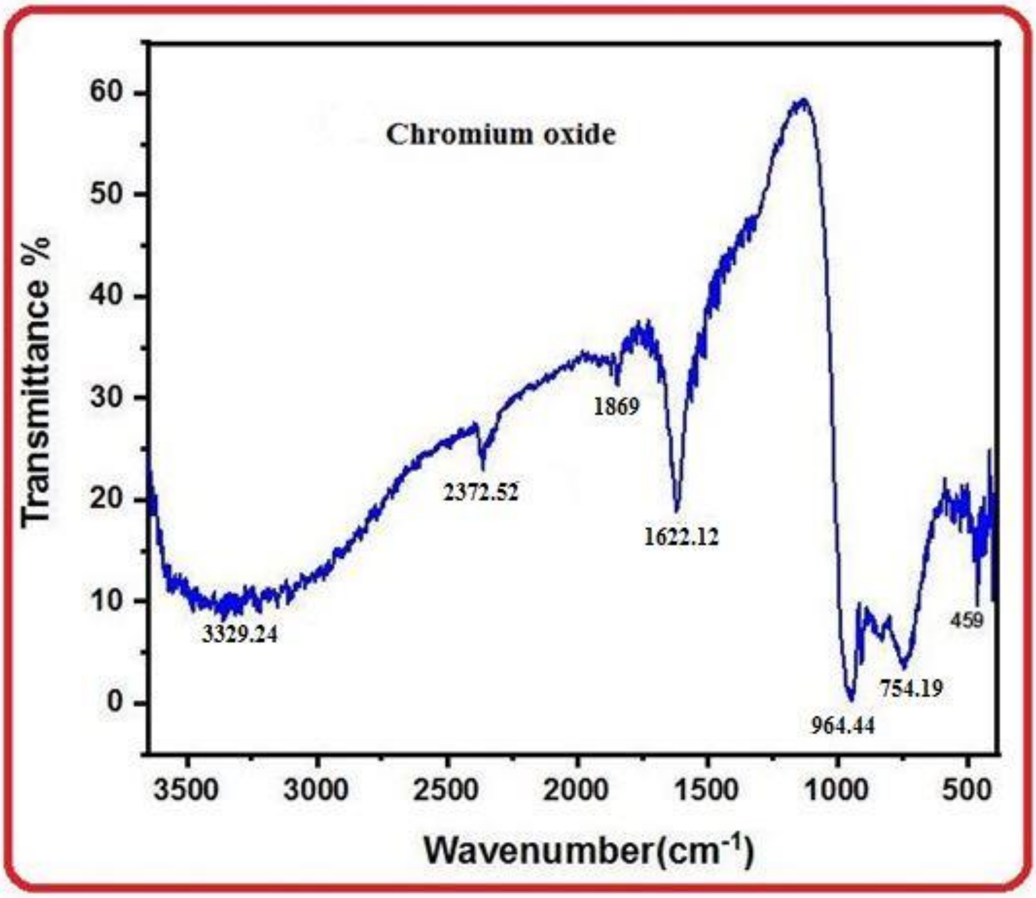

Fig. (3-5): FTIR spectra of Chromium oxide nanoparticles

3-1-4-3- FTIR spectra Cr_2O_3\ZnO nanocomposite.

FTIR spectroscopy of Cr_2O_3\ZnO nanocomposite was carried out using (Perkin Elmer model 1650) over the range of 400–4000 cm^{-1} FTIR spectra of Cr_2O_3\ZnO nanocomposite consists of the peaks at (433,516.93,623.02,970.22,1060,1543,2366.73, and 3439.19 cm1). The stretching vibrations of the (OH) groups are represented by the absorption peak, which was seen at 3439.19 cm1. Groups (C-H) are represented by the band at 2366.73 cm1. The band located at 1543 cm^{-1} represented (CO_2) symmetric groups. The peak at 1060 cm^{-1} can be attributed to the (C-O-C) bond ,970.22 (Cr-O) strong vibration,623.02(Cr-O),516.93 (Zn-O) and 433 cm^{-1} (Cr-O)). (Mohamed et al., 2019) All results are in Figure. (3-6).

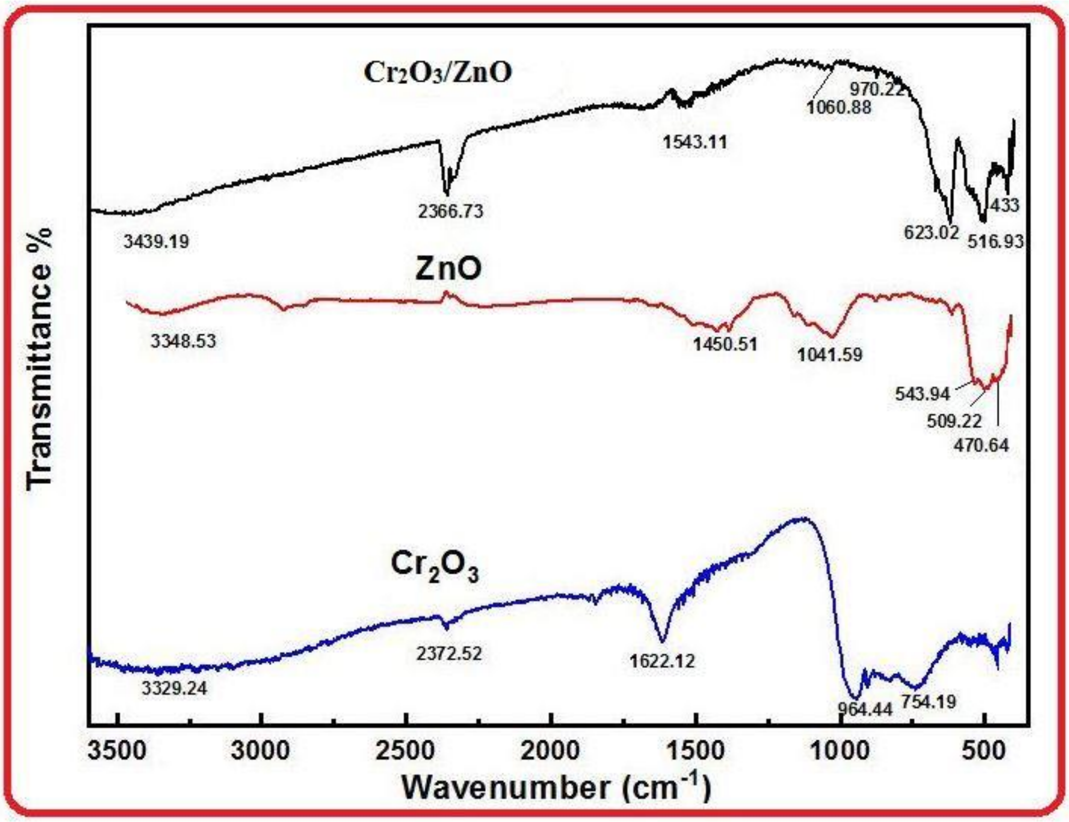

Fig. (3-6): FTIR Spectra ZnO, Cr_2O_3,Cr_2O_3\ZnO nanocomposite.

3-1-5- Scanning Electron Microscopy (SEM) for synthesized Cr_2O_3\ZnO nanocomposites.

Scanning Electron Microscopy techniques(SEM, Zeiss, Germany) was used to investigations the surface morphological of the Cr_2O_3/ZnO nanocomposite particles,in order to obtained useful catalyst. SEM images, Gaussian and histogram of Cr_2O_3/ZnO nanocomposite are illustrated in Figure. (3-7). SEM micrograph analysis was appeared as irregular distributed aggregated along with aspherical shape. The average grain size measured from histogram was in the range of (10-20nm), and the grain size equal (13.63 nm) from Gaussian (Zelekew et al 2021) (Ainali et al., 2021).

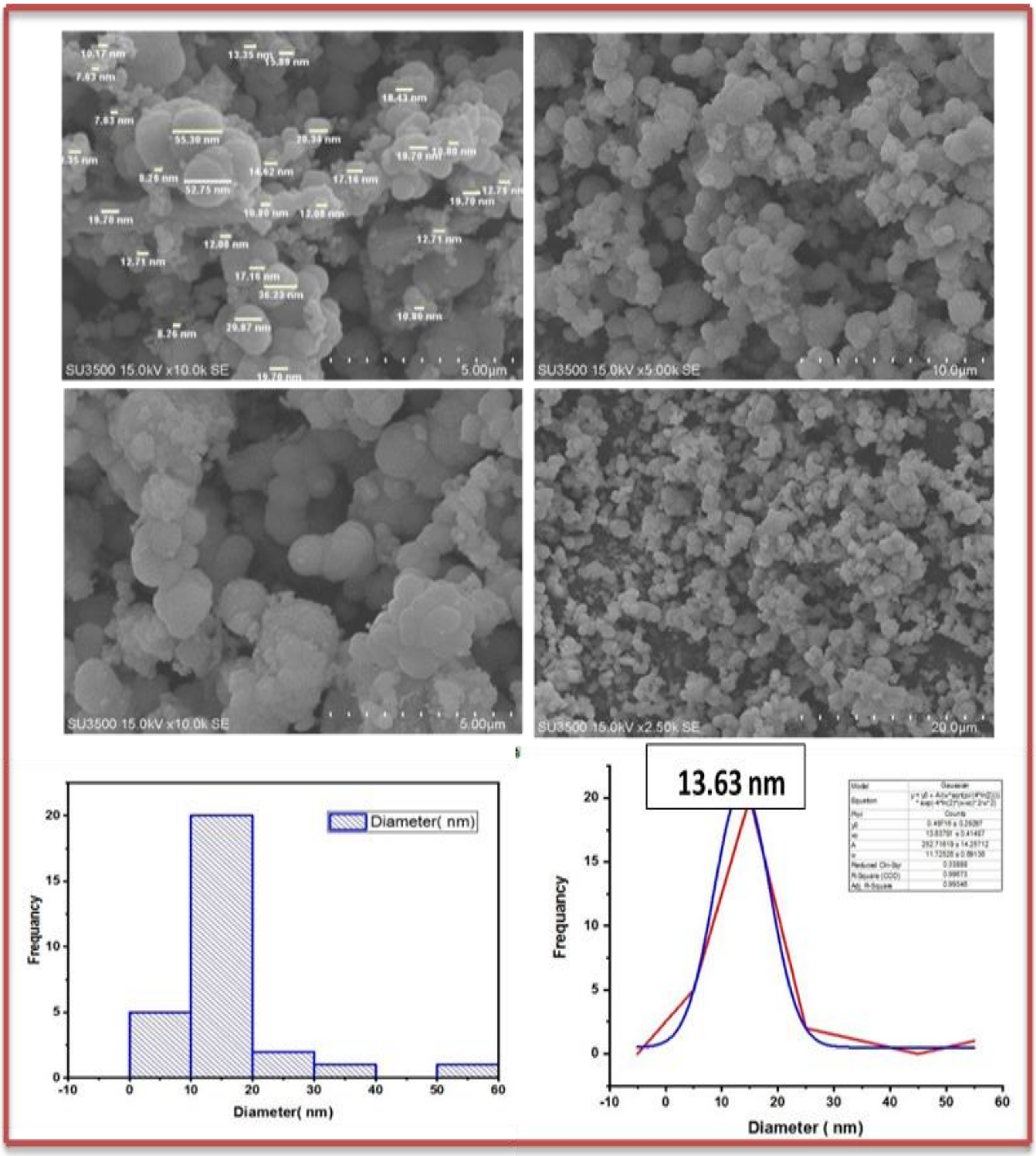

Fig. (3-7): SEM pattern of Cr_2O_3\ZnO nanocomposite.

3-1-6 Thermo Gravimetric Analysis (TGA) for Cr_2O_3\ZnO nanocomposite:

TGA is an analytical technique, was used to determine the temperature decomposition of metal precursors using the NETZSCH STA 2500 TGA setup, which operates at room temperatures up to (800 °C). Thermal properties of Cr_2O_3/ZnO nanocomposite were investigated using Thermogravimetric analysis(TGA), the sample weighed approximately (10 mg) and was placed inside a platinum crucible with air or nitrogen flowing at a rate of (20 cm3 min–1). As clear in Figure. (3-8) a major weight loss (60 mg) was observed in the range (100 – 200°C), this weigh loss which is due to evaporation of the water on the surface of the nanocomposites, after that the nanocomposite stables at 600°C (Badvi et al., 2021) (Wani et al., 2021)

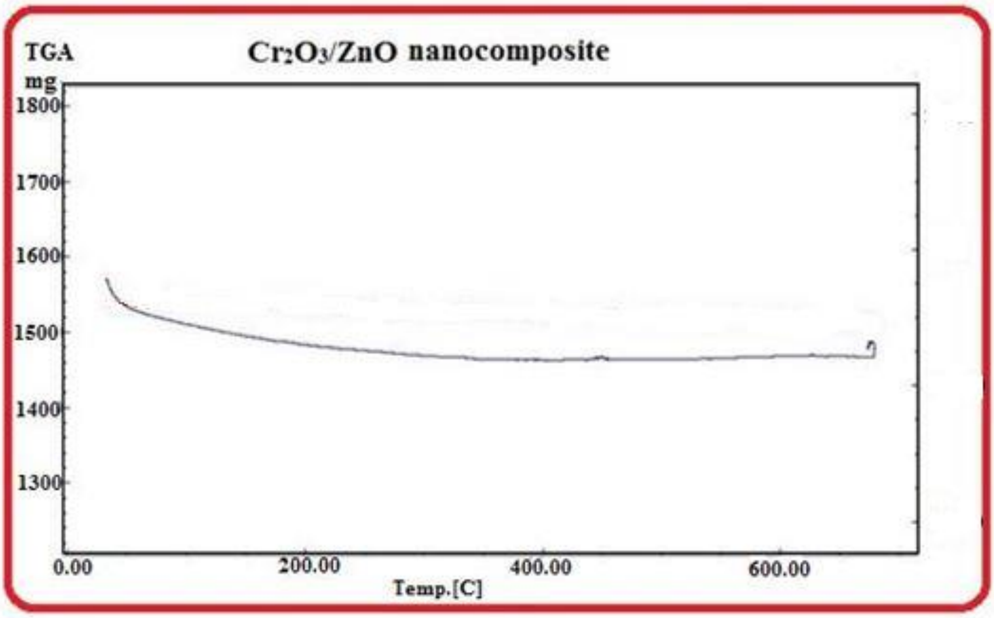

Fig. (3-8): Thermogravimetric analysis (TGA) of Cr_2O_3\ZnO nanocomposite.

3-1-7 UV-Diffuse Reflectnce Cr_2O_3\ZnO Nanocomposite :

The band gap of synthesized Cr_2O_3\ZnO nanocomposite was calculated using Kubelka-Munk method, by plotting $(F(R)h\nu)^2$ versus Energy (eV). The energy gap can be determination by exterapolting the strainght line. The result were shown in Fig. (3-9). The obtained absorption band edge was at approximately 333.23 and 398.70 nm. bonding between ZnO and Cr_2O_3 lead to a shift the band gap of the ZnO nanoparticle from 3.37 eV to 2.8 eV (Reda et al., 2021).

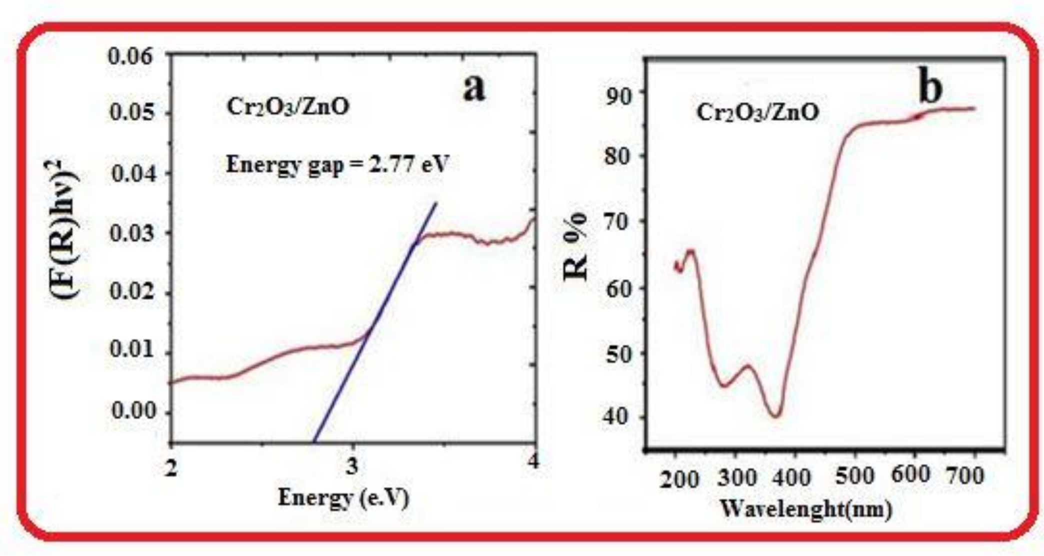

Fig. (3-9): (a) Kubela-Munk Plots for Cr_2O_3/ZnO nanocomposite at 600°C, and (b) Diffuse-reflectance UV-visible spectrum of Cr_2O_3/ZnO nanocomposite at 600°C

3-2 Photocatalytic degradation of fuchsin acid dye

3-2-1-A Preliminary experiments

Many experiments were performed to reach the optimum conditions of the photocatalytic degradation processes. The first reaction has been done using (20mg/L) of fuchin acid dye with the addition (0.13 g/100mL) of

Cr_2O_3/ZnO nanocomposite under mearcury lamp,(10ml/min) flow rate of air at room temperature (25°C) and (pH=9) (photocatalytic process). The second reaction has been carried out using (20mg/L) of dye in the dark using (0.13 g/100mL) of Cr_2O_3/ZnO nanocomposite , (10ml/min) flow rate of air at room temperature (25°C) and (pH=9) (adsorption). Third reaction was performed using the same solution but without addition of Cr_2O_3/ZnO nanocomposite under mearcury lamp (photolysis). As shown in Figure. (3-11), photocatalytic process gave the best degrade of the polluting dye(fuchsin acid dye) compared to the adsorption process, followed by the photolysis process(photocatalytic process>Adsorption process> photolysis process). (Zelekew et al., 2021).

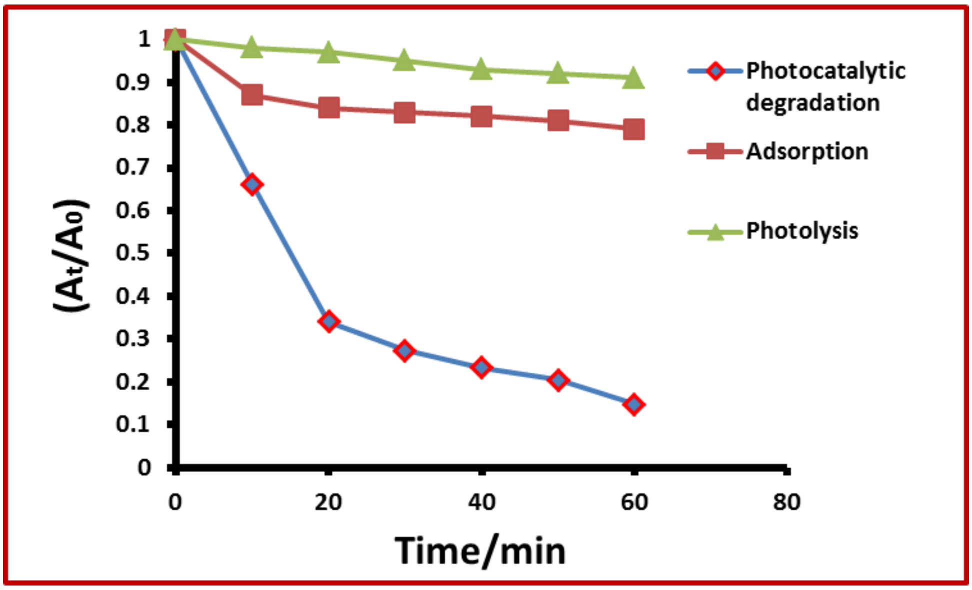

Fig. (3-10): Variation in (A_t / A_0) with irradiation time at (20 mg/L) of fuchsin acid dye and 0.13 g/100mL of catalyst.

3-2-1-B Comparison betweenZnO nanoparticles and Cr_2O_3/ZnO nanocomposite

Different experiments have been performed for studing the photocatalytic activity of synthesized ZnO nanoparticles and Cr_2O_3/ZnO nanocomposite using fuchsin acid dye under UV light irradiation. In this process

0.13g/100mL amount of catalyst (ZnO nanoparticles and Cr_2O_3/ZnO nanocomposite separately) was added into 100 mL of an aqueous solution of fuchsin acid dye at a constant initial concentrations of 20mg/L .

As shown in Figure (3-11) Cr_2O_3/ZnO nanocomposite(82.32%) is better photocatalyst than ZnO (75.67%) for degradation of fuchsin acid dye.

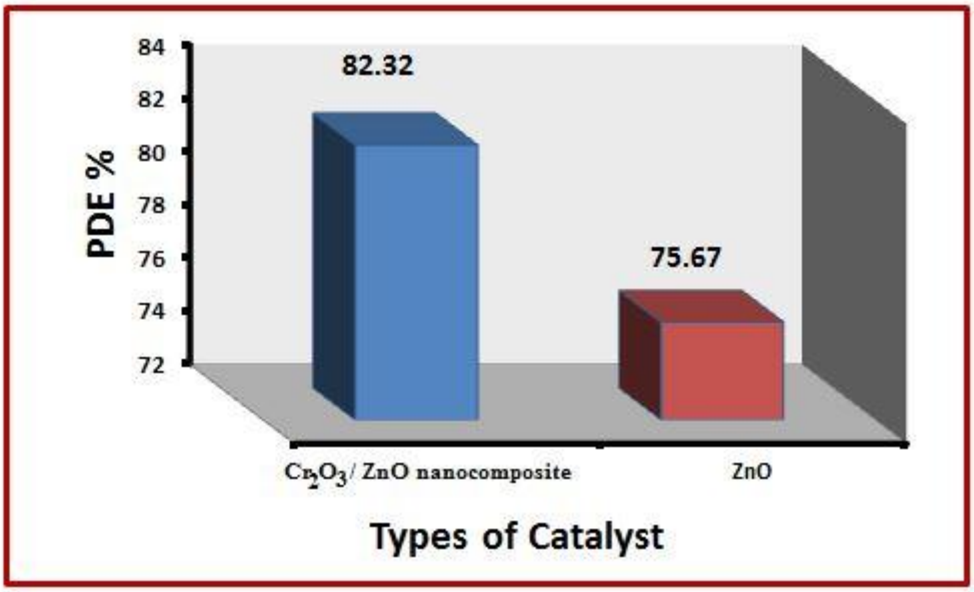

Fig. (3-11): Photocatalytic degradation efficiency using (20mg\L) of fuchsin acid,pH=9.0, and 10mL/min flow rate of air, against different catalyst.

3-2-2 The Effect of different parameter on the photocatalytic degradation for fuchsin acid dye.

The photocatalytic degradation efficiency of fuchsin acid dye will depend on diferent parameter that affects on the surface properties of Cr_2O_3/ZnO nanocomposite. (Niu et al., 2020) (Rashid et al., 2016).

3-2-2-1 The Effect of the mass of Cr_2O_3\ZnO nanocomposite on photo catalytic degradation of the fuchsin acid dye

The effect of masses of Cr_2O_3/ZnO nanocomposite on Photocatalytic degradation of fuchsin acid dye, was studied .using (20 mg/L) of dye, flow rate of air (10mL/min), temperature (25°C) and (pH=9). Cr_2O_3/ZnO nano-composite heterogeneous nanostructure was used in different weight amounts (0.03,0.06,0.13.and0.2g/100mL), by keeping dye concentration as constant at 20 mg/L at pH 9.0and 10mL/min at 298k.As shown in Table (3-4) and Figure (3-12), (3-13).,The photocatalytic degradation increases up to 0.13g/100mL of nanostructure catalyst in 100 ml of the fuchsin acid dye solution due to increase in the reactive sites on the Cr_2O_3/ZnO nanocomposite, beyond 0.13g/100mL of nanostructure catalyst the degradation process is reduced, because of the scattering of light and decrease in the penetration of light in the dye solution for the reaction.When the amount of catalyst is higher in the solution, lead to increases the turbidity of the dye solution and reduce the penetration of light, and thereby leads to the decrease in the photocatalytic degradation of dye. Also, the surface area becomes less as a result of nanocomposite agglomeration at higher concentration of Cr_2O_3/ZnO nanocomposite. (Alshehri et al., 2020) (Jamil et al., 2020).

Table (3-4): The chang in (A_t\A_0) with irradiation time on different masses of Cr_2O_3\ZnO nanocomposite.

Catalyst mass of (Cr_2O_3/ZnO) g/100ml	0.03	0.06	0.13	0.20
Irradiation Time/min	A_t/A_0			
0	1	1	1	1
10	0.95	0.84	0.56	0.77
20	0.89	0.72	0.33	0.59
30	0.74	0.65	0.26	0.49
40	0.71	0.56	0.26	0.38
50	0.66	0.53	0.23	0.33
60	0.66	0.52	0.18	0.34

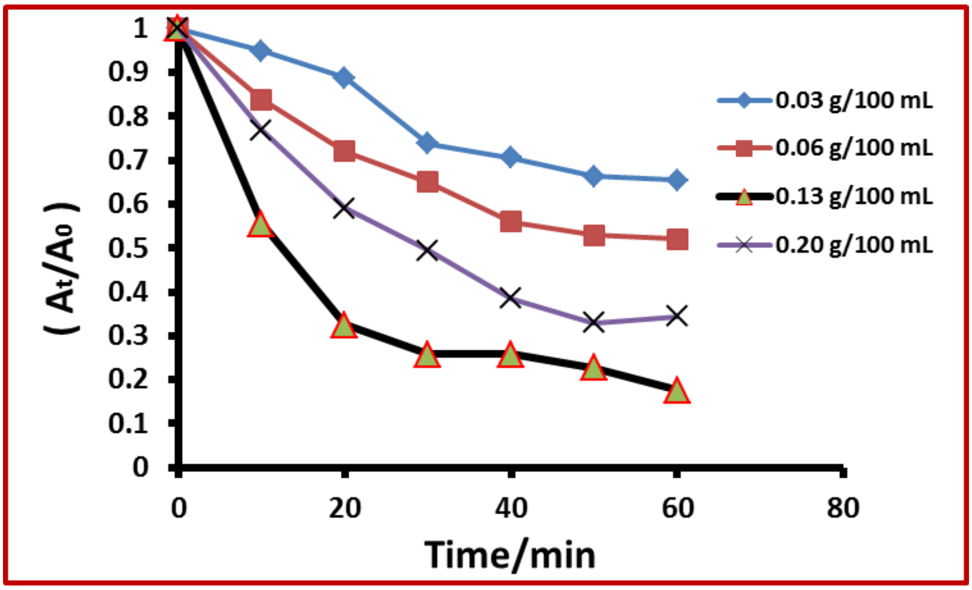

Fig. (3-12): Variation in (A_t \ A_0) with irradiation time at (20 mg\L) of fuchsin acid dye,pH=9.0,and 10mL/min flow rate of air.

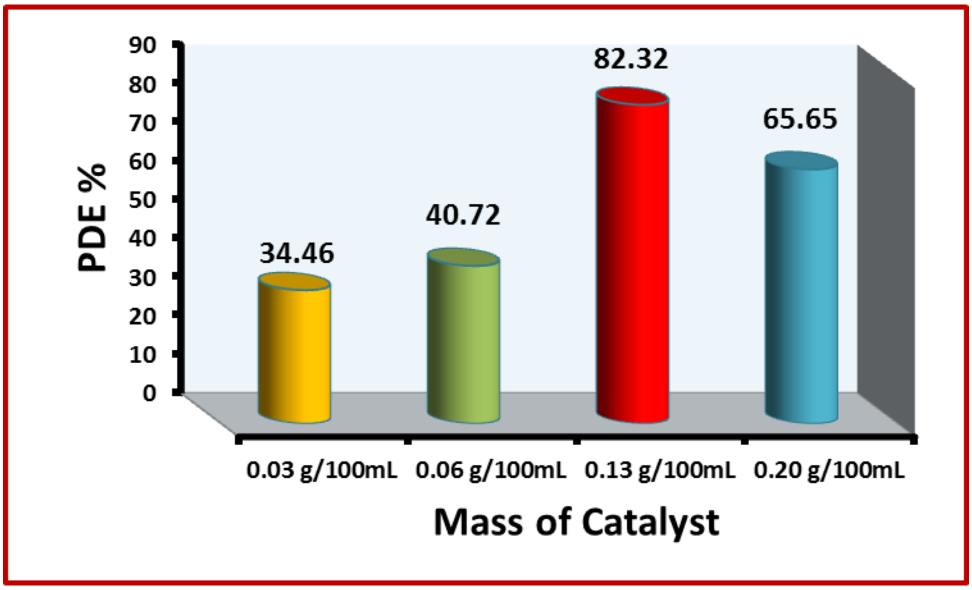

Fig. (3-13): Photocatalytic degradation efficiency using (20mg\L) of fuchsin acid,pH=9.0, and 10mL/min flow rate of air, against masses of Cr_2O_3\ ZnO nanocomposite.

3-2-2-2 Effect of fuchsin acid dye initial concentration on the photocatalytic degradation process

The effect of fuchsin acid dye concentration solution in the photocatalytic degradation processes (20,30,40,and70 mg\L) was tested by keeping all the other experimental conditions constant at temperature (298k), flow rate of air (10mL\min), (pH=9.0) and 0.13 g/100mL mass of Cr_2O_3\ZnO nanocomposite. The results are plotted in Table (3-5) and Figure (3-14), (3-16). These results indicated that the photocatalytic degradation of dye reduced with the increasing of initial dye concentration. As initial fuchsin acid dye concentration decreases, the path length of the photon entering the suspension solution decreases so the number of photons reaching to Cr_2O_3\ZnO nanocomposite surface increase and hence rate of formation hydroxyl radicals and super oxide ions are increased, thereby increasing rate of degradation (Mondol et al., 2021).

Table (3-5): change of$A_t \backslash A_0$ through irradiation-time on different concentration for fuchsin acid dye.

oncentration of fuchin acid dye (mg/L)	20	30	40	70
Iradiation Time min	A_t/A_0			
0	1	1	1	1
10	0.70	0.82	0.90	0.92
20	0.46	0.63	0.79	0.83
30	0.27	0.42	0.66	0.75
40	0.23	0.39	0.51	0.64
50	0.21	0.33	0.52	0.63
60	0.15	0.29	0.51	0.56

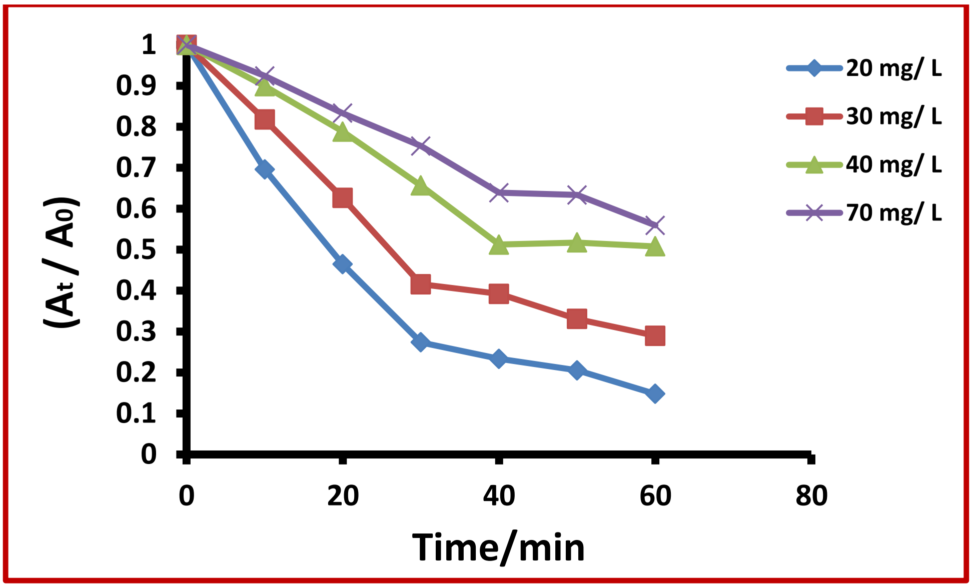

Fig. (3-14): Variation in ($At \backslash A_0$) with irradiation time at different concentrations of fuchsin acid dye,0.13g/100mL, pH=9.0,and 10mL/min flow rate of air.

Langmuir–Hinshelwood rate expression has been successfully used for heterogeneous photocatalytic degradation to determine the relationship between the initial degradation rate and the initial concentration of the organic substrate. The Langmuir-Hinshelwood madel is experessed as Eq.(2-6)and (2-7)

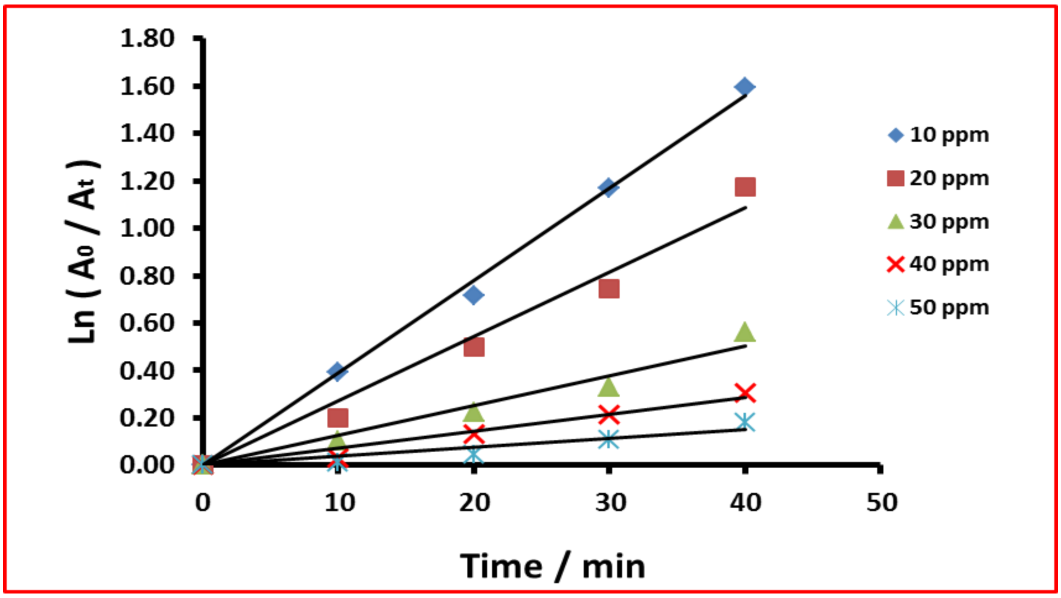

Fig.(3-15): Linear variation of ln(A_0 \A_t) versus time for the photocatalytic degradation of fuchsin acid dye at different initial concentrations,0.13g/100mL, pH=9.0,and 10mL/min flow rate of air.

The results showed that the kinetics of photocatalytic reaction fit the Langmiur– Hinshelwood kinetics model well. Therefore, the absorption of fuchsin acid on the thin film surface is the controlling step in the whole degradation process Figure (3-15).

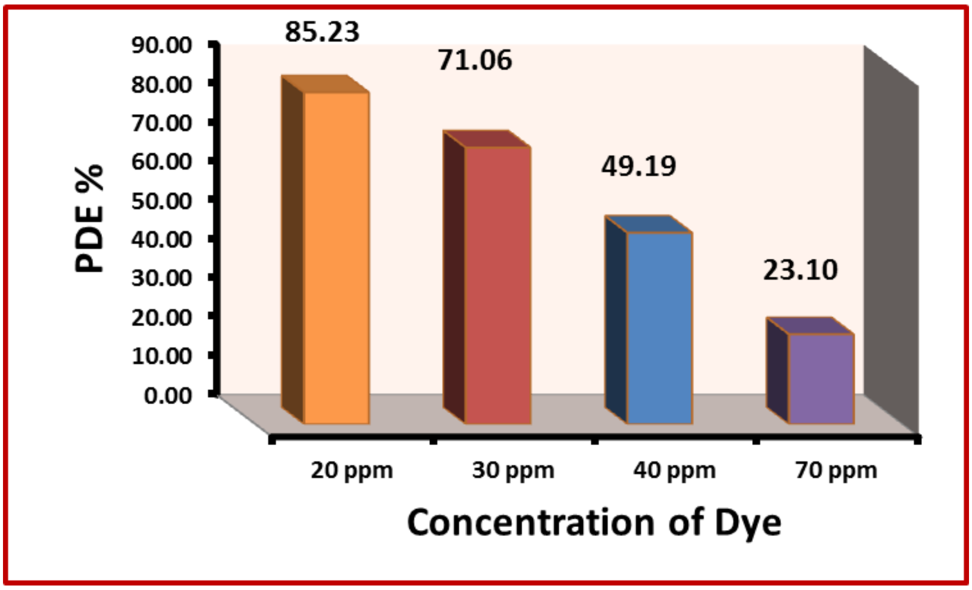

Fig. (3-16): Photocatalytic degradation efficiency at different concentration of fuchsin acid dye. using 0.13 g \ 100 mL Cr_2O_3\ ZnO nanocomposite, pH=9.0,and 10mL/min flow rate of air.

3.2.2.3 : The Effect of the hydrogen Peroxide on photocatalytic degradation of fuchsin acid dye.

Different experiments were performed for study the effect of the initial hydrogen peroxide concentration (0.098 ,0.196 ,0.293 and 0.392M) on the photocatalytic degradation of fuchsin acid dye using 0.13 g\100 mL Cr_2O_3\ZnO naocomposite , 20 mg\L initial concentration of fuchsin acid dye,pH=9.0 and 10 mL\min flow rate of an air bubble at temperature 298k. Table (3-6) and Figure. (3-17) shows the effect of hydrogen peroxide concentration on photocatalytic degradation of dye.As shown in Figure (3-17), (3-18) degradation efficiency enhanced from (21.11 to 91.66%) by increasing the initial hydrogen peroxide concentration from (0.098 to 0.292M). The increases in photocatalytic degradation efficiency of fuchsin acid after the addition of hydrogen peroxide due to the increased reaction between hydrogen peroxide and electron in the conduction band, on the other hand hydrogen peroxide can effectively inhibit the electron–hole recombination. Since hydrogen peroxide is a better electron acceptor than dissolved oxygen, it could act as an alternative electron acceptor to oxygen. At low concentration of hydrogen peroxide, inhibition of the electron–hole recombination is effectively contributed to the photocatalytic degradation of fuchsin acid dye. However, further increase in hydrogen peroxide concentration above (0.293M) caused lower degradation of fuchsin acid due to an inhibitive effect on the reaction between fuchsin acid and electron in the conduction band of Cr_2O_3\ZnO nanocomposite. The other reason for the inhibition effect can also be explained in terms of scavenging of positive holes by adsorbed H_2O_2 on the surface of Cr_2O_3\ZnO nanocomposite (Danyliuk et al., 2021) (Aziztyana et al., 2019) (Sharma et al., 2021). The added H_2O_2 could accelerate the reaction by producing hydroxyl radicals from scavenging the electrons and absorption of UV-light by the following reactions:

$$\mathbf{H_2O_2 + e^-_{(c.b.)} \rightarrow {}^{\bullet}OH + {}^{-}OH} \quad \mathbf{(3\text{-}3)}$$

$$\mathbf{H_2O_2 + O_2^{\bullet -} \rightarrow {}^{\bullet}OH + {}^{-}OH + O_2} \quad \mathbf{(3\text{-}4)}$$

$$\mathbf{H_2O_2 + h\nu \rightarrow 2{}^{\bullet}OH} \quad \mathbf{(3\text{-}5)}$$

By addition of excess **H_2O_2**, it acts as hydroxyal radical or hole scavenger to form the perhydroxyl radicals **($HO_2^{\bullet}$)** which is a much weaker oxidant than hydroxyl radicals **:**

$$\mathbf{H_2O_2 + {\bullet}OH \rightarrow H_2O + HO_2^{\bullet}} \quad \mathbf{(3\text{-}6)}$$

$$\mathbf{H_2O_2 + h^+ \rightarrow H^+ + HO_2^{\bullet}} \quad \mathbf{(3\text{-}7)}$$

Table (3-6): change for$A_t\backslash A_0$ through irradiation-time on different initial H_2O_2 solution value.

initial hydrogen Peroxide solution % v/v	0.098M	0.196M	0.293M	0.392M
Iradiation Time min	A_t/A_o			
0	1	1	1	1
10	0.95	0.90	0.60	0.71
20	0.87	0.79	0.47	0.58
30	0.84	0.65	0.25	0.44
40	0.72	0.57	0.19	0.40
50	0.68	0.45	0.14	0.29
60	0.66	0.42	0.08	0.25

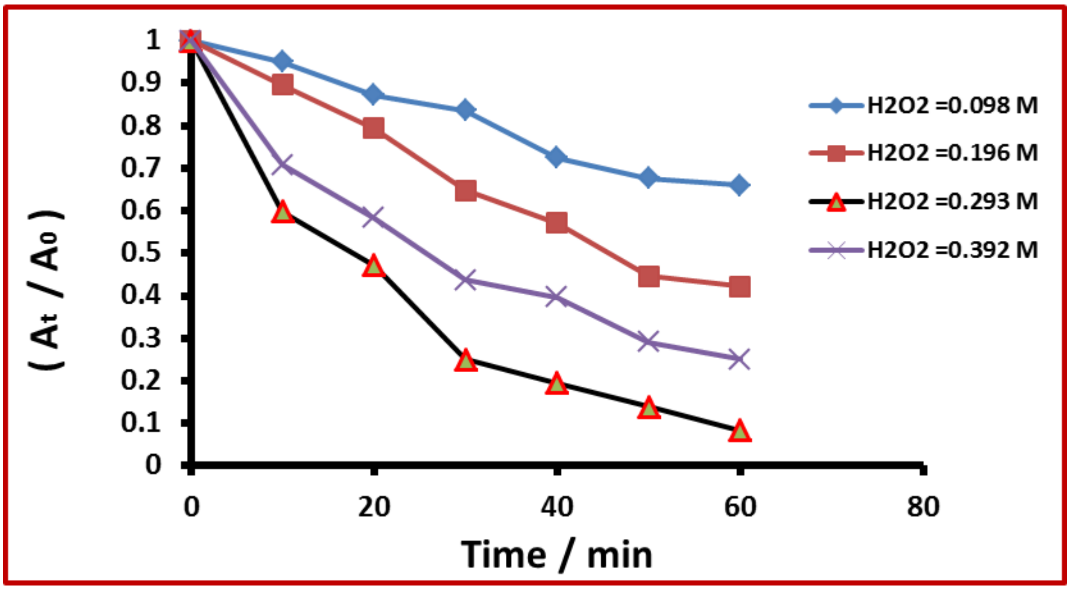

Fig. (3-17): Variation in (A_t \ A_0) with irradiation time at different initial H_2O_2 solution, using (0.13g / 100 mL) Cr_2O_3/ZnO nanocomposite and (20 mg/L) of fuchin acid dye .

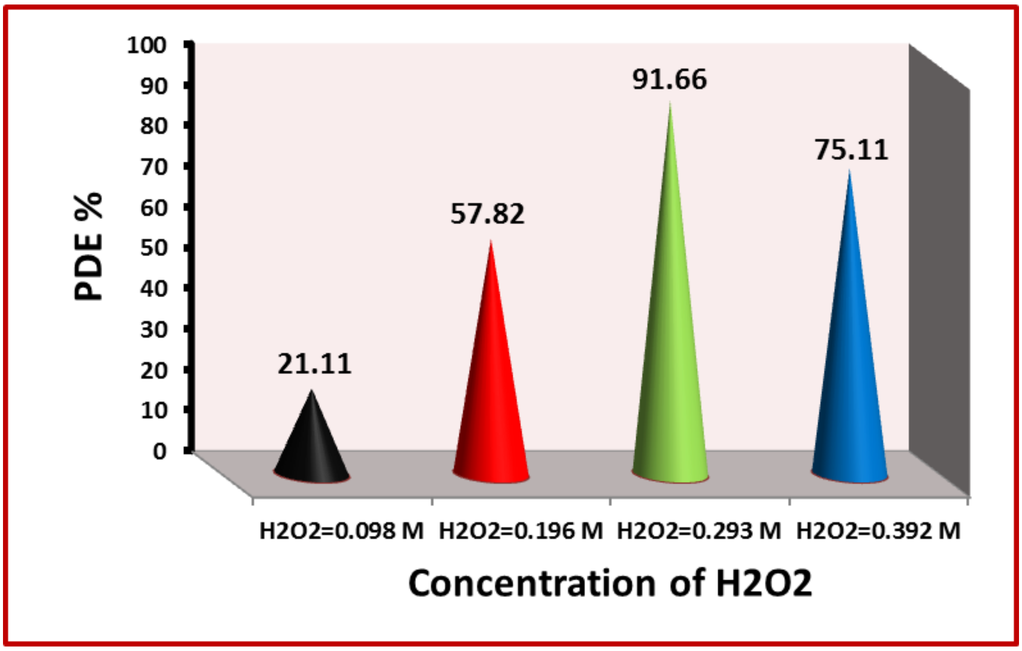

Fig. (3-18) . Photocatalytic degradation efficiency using (0.13g / 100 mL) Cr_2O_3/ZnO nanocomposite and (20 mg/L) of fuchin acid dye for different H_2O_2 concentrations

3-2-2-4 Effect of pH on photocatalytic degradation of fuchsin acid dye:

A set of experiments was performed to investigate the effect of initial pH of suspension solution on the ability photocatalytic degradation of fuchsin acid dye over 0.13 g \100mL of Cr_2O_3\ZnO nanocomposite, 20mg\L of fuchsin acid dye concentration, (10 mL\min) flow rate of an air bubble at temperature 298k. The practical experiments were carried out under pH solution (4, 5, 9 and 10). As shown in Table (3-6) and Figure (3-19), (3-20) ,the optimum value of degradation fuchsin acid dye, was determined at (pH=9). At pH in the acidic medium the surface of catalyst become acidic this lead to increase repulsion of dye molecules with catalyst surface, and hence decreases photocatalytic degradation efficiency (Abilarasu et al., 2021).

Table (3-7): change for at\A_0 through irradiation-time on diffrent pH value.

Initial-pH solution	4	5	9	10
Iradiation Time /min	A_t/A_o			
0	1	1	1	1
10	0.86	0.96	0.66	0.80
20	0.71	0.88	0.54	0.68
30	0.58	0.73	0.37	0.52
40	0.43	0.69	0.31	0.36
50	0.37	0.49	0.21	0.32
60	0.34	0.39	0.11	0.21

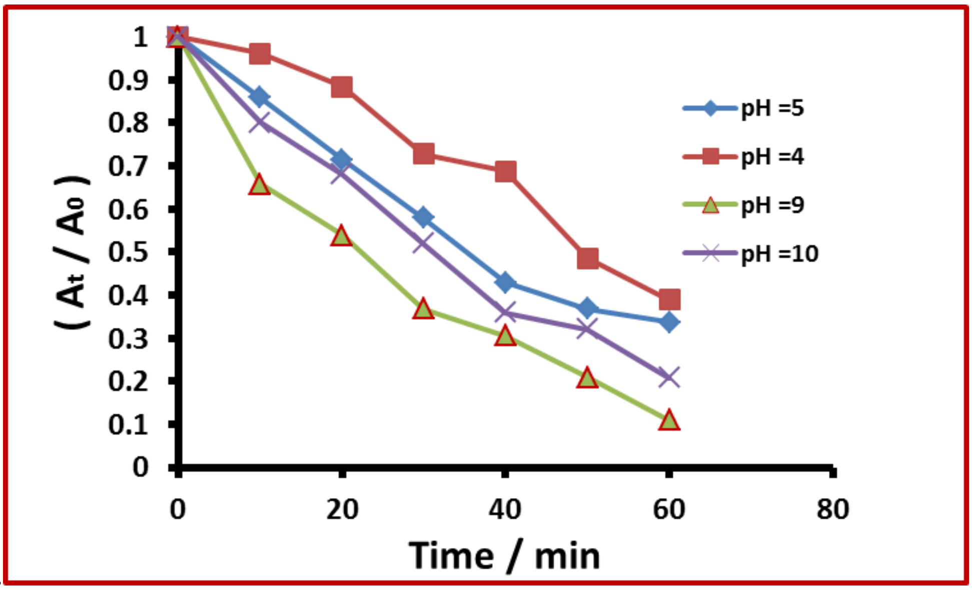

Fig. (3-19): Change in ln (A_0 \ A_t) through irradiation-time at different pH using UV radiation, using (0.13g / 100 mL) Cr_2O_3/ZnO nanocomposite and (20 mg/L) of fuchin acid dye.

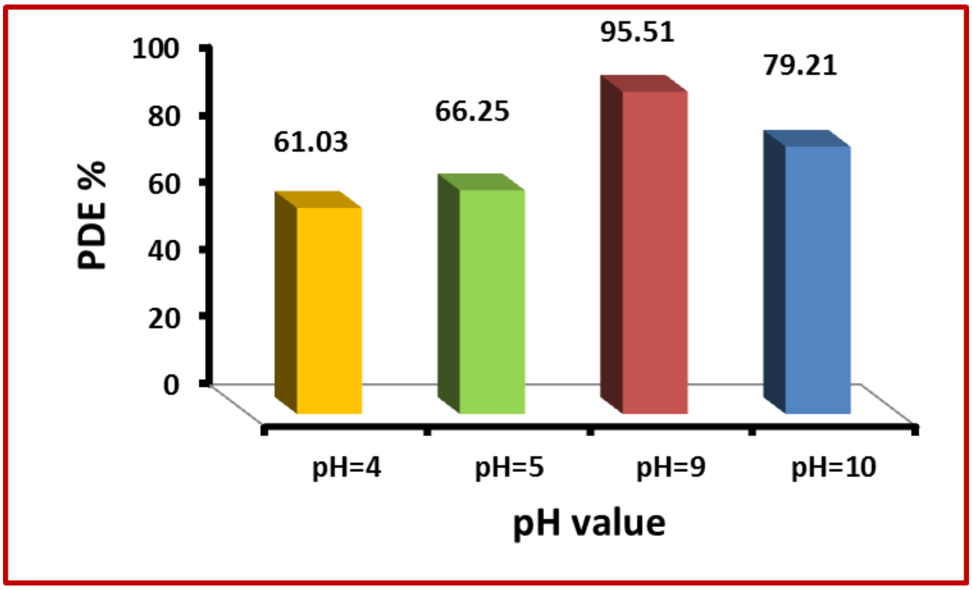

Fig. (3-20): Photocatalytic degradation efficiency using (0.13g / 100 mL) Cr_2O_3/ZnO nanocomposite and (20 mg/L) of fuchsin acid dye for different initial pH.

3-2-2-5 Investigation of different reactive oxidative species

The photodegradation of fuchsin acid dye by using Cr_2O_3 / ZnO nanocomposite has been investigated with the addition of three active scavengers' species, each scavenger specifies in trapping one active species. For example, Ascorbic acid, EDTA-Na and Sodium azide as being evaluation with the scavengers of superoxide radicals **($^{\bullet -}$ O_2)**, holes (h^+) and singlet oxygen $^1O_2$ respectively.

The results are shown in Figure (3-21), (3-22) when 1.2 mM of Sodium azide was added to fuchsin acid dye solution in the presence of Cr_2O_3 /ZnO nanocomposite, the degradation rate was decreases as 76.79%, which conclude that the main active species such as singlet oxygen $^1O_2$ is finely affected. While the degradation rate of fuchsin acid dye was decreased 55.19% with the addition of Ascorbic acid signifying that the superoxide radicals ($^{\bullet -}$ O_2) radical) plays a certain role in photocatalysis process.

When EDTA-Na was added, the degradation rate of fuchsin acid dye was highly affected, the degradation rate was decreases as 42.70%, representing that the holes (h^+).

Table (3-8): change for $A_t \backslash A_0$ through irradiation-time on diffrent Scavenging agent value.

scavenging agent	Blank	Sodium azide	Ascorbic acid	EDTA-Na
Iradiation Time min	A_t/A_o			
0	1	1	1	1
10	0.70	0.79	0.92	0.96
20	0.51	0.64	0.75	0.89
30	0.27	0.48	0.64	0.76
40	0.23	0.37	0.59	0.70
50	0.21	0.33	0.50	0.67
60	0.15	0.23	0.45	0.57

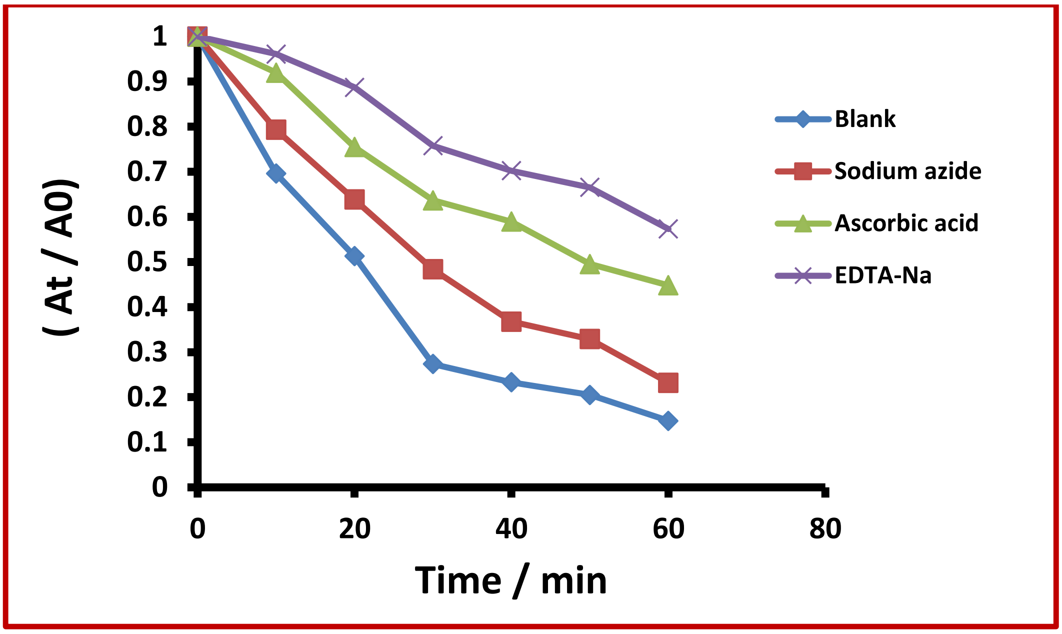

Fig. (3-21). Photodegradation rate in the presence of different scav-enging agent with precence Cr_2O_3/ZnO, using (0.13g / 100 mL) Cr_2O_3/ZnO nanocomposite and (20 mg/L) of fuchin acid dye

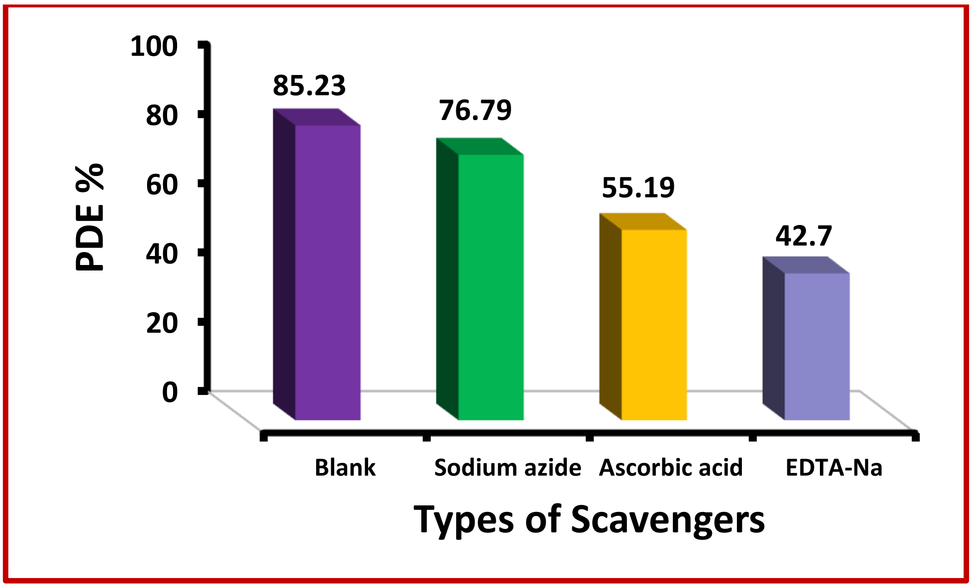

Fig. (3-22): Photocatalytic degradation efficiency using (0.13g \ 100 mL) Cr_2O_3\ ZnO nanocomposite and (20 mg\L) of acid fuchsin dye for different scavenger's agent.

3-2-2-6 The effect of Temperature on photocatalytic degradation of fuchsin acid dye:

A series of experiments were done for studding the influence of temperature on photocatalytic degradation of fuchin acid dye (288 ,298,303,and 308) k. By conservation other experimental conditions apply constant at 20 mg\L initial fuchsin acid dye concentration of (0.13 g \100mL) prepared Cr_2O_3 /ZnO nanocomposite dosage , (10 mL\min flow rate of an air bubble ,and pH=9.0. The results in Table (3-9) and Figure (3-23), (3-24) show that the degradation process of dye progressively increased with increase in the temperature, this due to the increased reactive hydroxyl radical obstetrics (Singh et al., 2021). The activation energy associated with the photodegrdation of dye was calculated according to the Arrhenius equation (2-7), by ploting of ln k versus 1\T. From Figure (3-25) the activation energy which equal 35.35. ±1 $kJ.mol^{-1}$.

Table (3-9): Change of $A_t \backslash A_0$ through irradiation-time of different-temperature.

Temperature /K	288	298	303	308
Irradiation Time/ min	A_t / A_0			
0	1	1	1	1
10	0.97	0.82	0.70	0.59
20	0.80	0.68	0.54	0.36
30	0.77	0.58	0.43	0.29
40	0.73	0.50	0.23	0.09
50	0.59	0.33	0.21	0.05
60	0.52	0.28	0.15	0.02

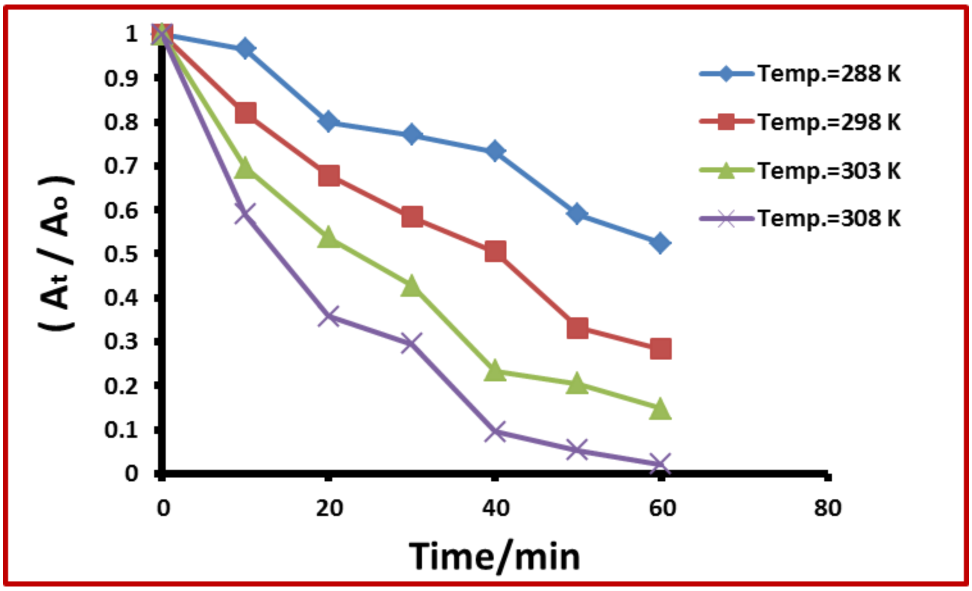

Fig. (3-23). Variation in ($A_t \backslash A_0$) with irradiation time at different temperature, using (0.13g / 100 mL) Cr_2O_3/ZnO nanocomposite and (20 mg/L) of fuchin acid dye

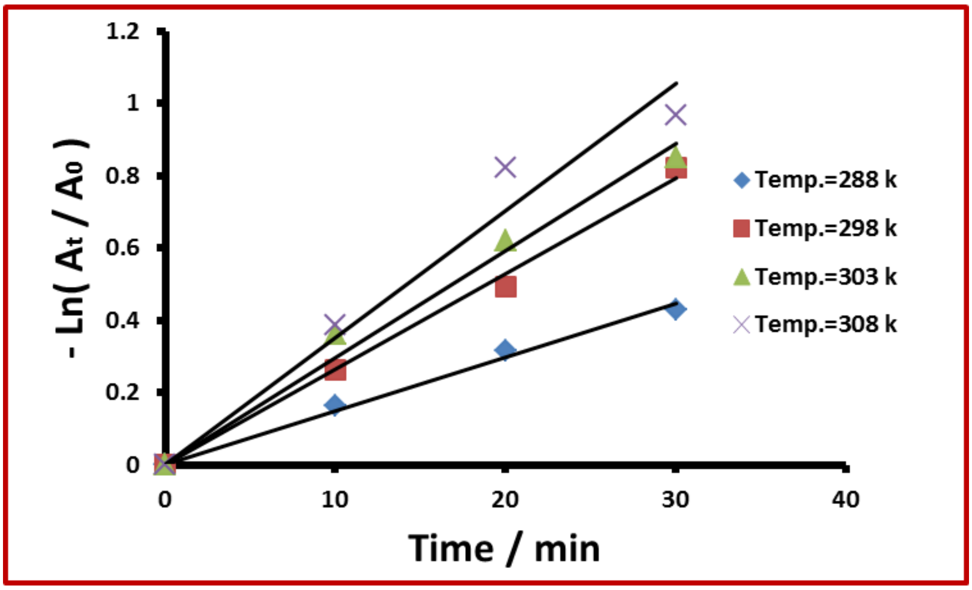

Fig. (3-24): Change in Ln (A_0 \ A_t) through irradiation-time at different-temperature using UV radiation, (20 mg\L) of fuchsin acid dye and (0.13g \ 100 mL) Cr_2O_3\ZnO nanocomposite.

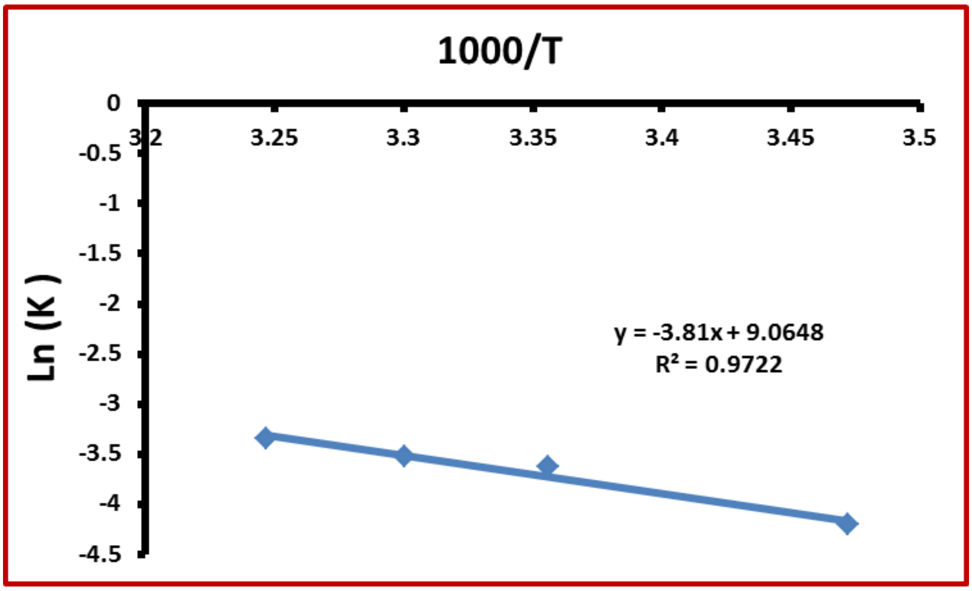

Fig. (3-25): Arrhenius plot of fuchsin acid dye.

In order to calculate thermodynamic functions such as ΔH (Change Enthalpy of activation) and ΔS (Change Entropy of activation), Figure (3-26) was shown a linear relationship fitting the graph of Eyring equation (2-8).

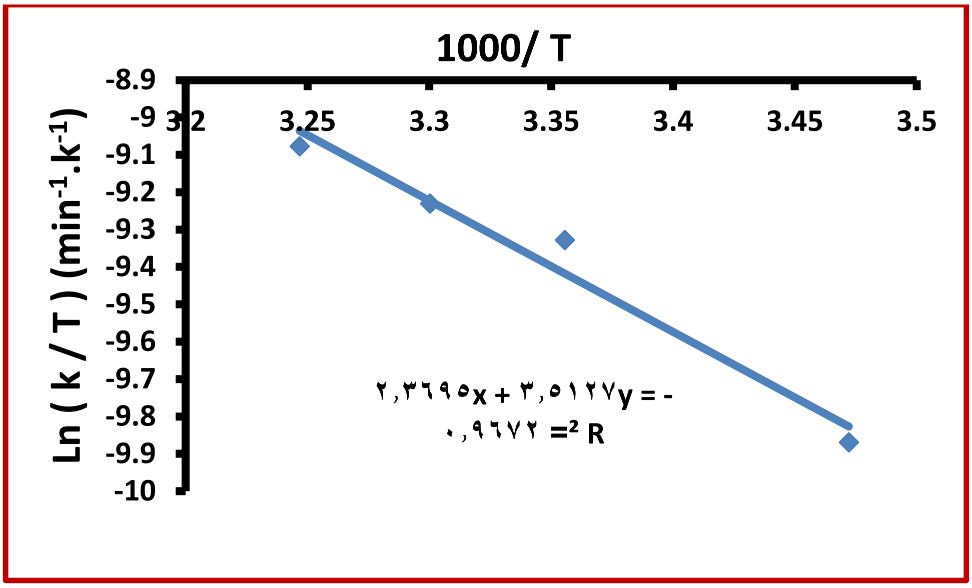

Fig. (3-26): Eyring equation plot ln(k\T) against 1000\T for fuchsin acid dye.

According to the equation (2-10), a plot of ln(k\T) versus 1\T produces a straight line and the value of Enthalpy of activation can be calculated from the slop of this line (ΔH=29.20 kJ\mol). And from the y-intercept the Entropy of activation value (ΔS=−0.1778k J\ mol. k).The positive value of Enthalpy of activation refers to endothermic reaction. In the present case the value of Entropy of activation is negative as in Table (3-10), so that the prodect formed is more ordered than the reactants. The Gibbs' free energy ΔG can be calculated from the equation (2-9) and equal (82.18 kJ\mol). The positive values of ΔG for the reaction indicate the non-spontaneous nature of photocatalytic degradation of fuchin acid dye.

Table (3-10): The thermodynamic parameters of the photocatalytic degradation of dye.

Temperature/ K	Enthalpy of activation/ $KJ.mol^{-1}$	Entropy of activation/ $KJ.mol^{-1}.k^{-1}$	Gibbs' free energy/ $kJ.mol^{-1}$
298	**29.20**	**- 0.1778**	**82.18**

3.3. Reaction kinetics

The rate of reaction has been studied using the effect of initial dye concentration(20, 30, 40, and 70 mg/L) using 0.13g / 100 mLCr_2O_3/ZnO nanocomposite. a series of experiments has been performed to determine the rate of reaction. Pseudo first order and pseudo second order kinetic expressions were widely used by majority of the researchers today to describe the photocatalytic oxidation of pollutant. These models are expressed by the equations (2-12) and (2-13). (Mohammad et al., 2021). Best fitting kinetic model was chosen using linear regression method. Figures. (3-27) and (3-28) depict the kinetics of fuchsin acid degradation under UV catalytic activities by the Cr_2O_3/ZnO photocatalysts.

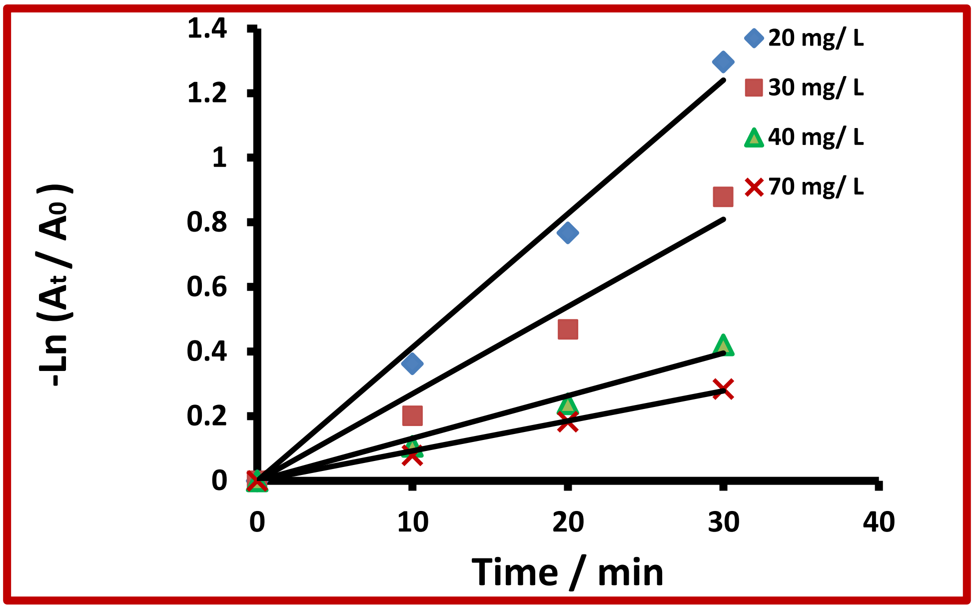

Fig. (3-27). The plots of ln (A_0 \A_t) versus irradiation time at different initial fuchsin acid concentrations. using0.13g / 100 mL Cr_2O_3/ZnO nanocomposite .

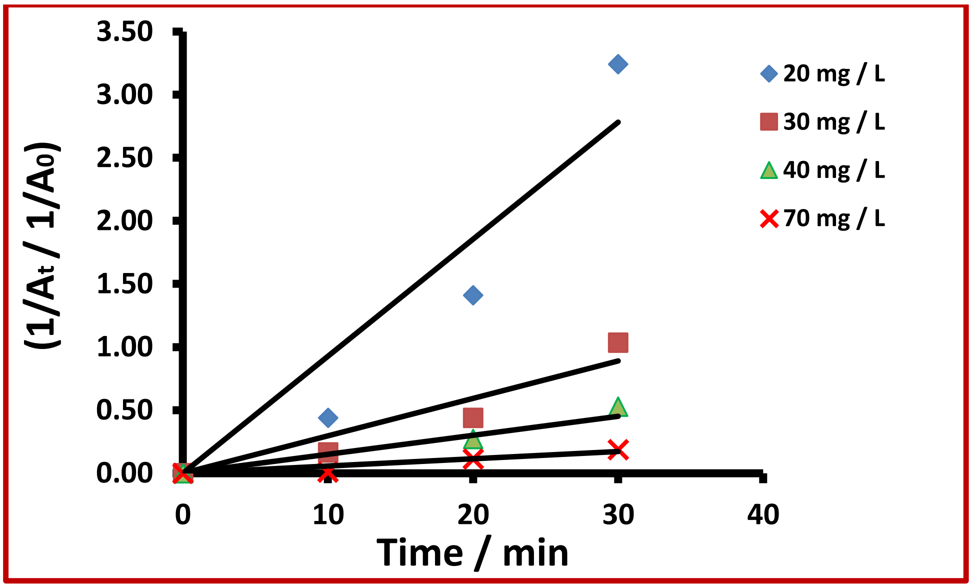

Fig. (3-28) : The plots of (1/A_t /1/A_0) with versus irradiation time at different initial fuchsin acid concentrations. using0.13g / 100 mL Cr_2O_3/ZnO nanocomposite .

Table (3-11) Kinetics of dye photo catalytic degradation by deferent concentration.

Concentration/ (mg/L)	First order		Second order	
	k_1	R^2	k_2	R^2
20	0.0093	0.995	0.0928	0.89857
30	0.0132	0.9806	0.0297	0.8996
40	0.027	0.9665	0.0151	0.8219
70	0.0413	0.9901	0.0057	0.8954

3-4 Proposed Mechanism of photocatalytic degradation of Fuchsin acid dye

When the aqueous fuchsin acid dye solution was exposed to UV light in the presence of Cr_2O_3/ZnO, the light irradiation promotes electron from valence band to conduction band of the chromium oxide leaving behind a positive hole(h+) in valence band as shown in Figure (3-29) . The photo generated electrons will move from the surface of p-type $Cr_2O_3$to the conduction band of the n-type ZnO and the holes will move to the valence band of the p-type Cr_2O_3. The electrons in the conduction band of ZnO will be interacted with oxygen and superoxide radical anions ($\bullet{-}O_2$) will be generated. Moreover, the holes in the valence band of the p-type Cr_2O_3 will be reacted with OH^- or H_2O and reactive oxygen species (•OH) will be formed. Then, •OH and $\bullet{-}O_2$ can be reacted with fuchsin acid dye and decomposition to H_2O and CO_2 is expected .

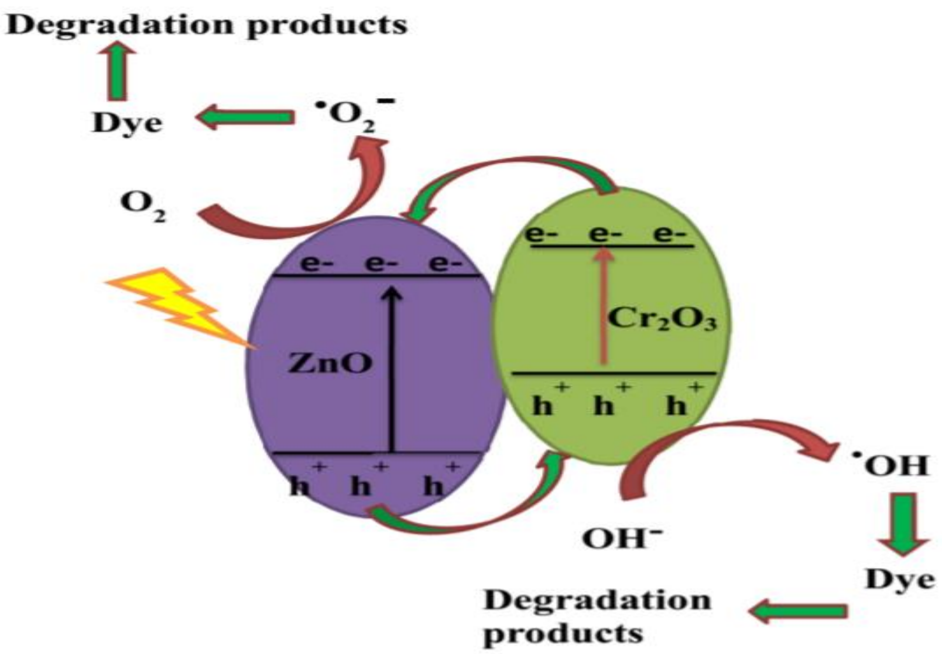

Figure. (3-29) Proposed photocatalyst under light irradiation mechanism of fuchsin acid dye with Cr_2O_3/ZnO nanocomposite.

The Cr_2O_3/ZnO nano composite photocatalyst mechanism is explained by the following equation:

$Cr_2O_3/ZnO + h\nu\ Cr_2O_3/ZnO \longrightarrow (e^-_{(CB)} + h^+_{(VB)})$ (3-6)

$Cr_2O_3/ZnO\ (e^-_{(CB)}) + O_2 \longrightarrow Cr_2O_3/ZnO + {}^{\bullet -}O_2$ (3-7)

$Cr_2O_3/ZnO\ (h^+_{(VB)}) + H_2O \longrightarrow Cr_2O_3/ZnO + H^+ + \bullet OH$ (3-8)

$Cr_2O_3/ZnO\ (h^+_{(VB)}) + {}^-OH \longrightarrow Cr_2O_3/ZnO + \bullet OH$ (3-9)

$Cr_2O_3/ZnO + {}^{\bullet -}O_2 +$ dye degrade dye $\longrightarrow (CO_2 + H_2O)$ (3-10)

$Cr_2O_3/ZnO + {}^{\bullet}OH +$ dye degrade dye $\longrightarrow (CO_2 + H_2O)$ (3-11)

3-5 Conclusions

1- Prepearation of Zinc Oxide nanoparticle using hydrothermal method. 2- Chromium oxide/Zinc Oxide (Cr_2O_3/ZnO) nanocomposite was pre- pared using hydrothermal method.

3-The mean crystallite size for the prepared Cr_2O_3/ZnO nanocomposite were calculated using Scherer equation, and the results showed that the average crystallite size and average particle size of all photocatalysts were 12.72 nm according to XRD.

4- The photocatalytic degradation processes of acid fusion dye depended on the amount of catalyst dosage and the optimum value equal (0.13 g / 100 mL) of Cr_2O_3/ZnO nanocomposite. The best photocatalytic degra- dation efficiency percentage of acid fusion dye (85.23%).

5- The effect of dye concentration has been studied the optimum value of acid fuchsin dye (20mg/L) dye. The photocatalytic degradation of acid fuchsin dye decrease with increase concentration of dye due to the decrease of the concentration OH^- adsorbed on the catalyst surface.

6- The activation energy has been calculated when used acid fuchsin dye = 31.67 $kJ.mol^{-1}$

8- Using Eyring equation thermodynamic parameters (ΔH, ΔS) for acid fuchsin dye were calculated (29.20 kJ/mol and (- 0.1778 kJ/mol. k) respectively, from the results the reaction is endothermic with low randomness. ΔG (82.18 kJ/mol) was calculated and the reaction is non-spontaneous.

9- Diferent materials has been used to quench the photocatalytic deg- radation process.

10- The Effect addition of the hydrogen peroxide concentration on photocatalytic degradation of dye. The increased photocatalytic degradation efficiency of acid fuchsin dye after the addition of hydrogen peroxide can be explained by the increased reaction between hydrogen peroxide and electron in the conduction band of acid fuchsin dye. According to, hydrogen peroxide can effectively inhibit the electron–hole recombination. The other reason for the inhibition effect can also be explained in terms of scavenging of positive holes by adsorbed H_2O_2 on the surface of Cr_2O_3/ZnO nanocomposite.

3-6 Recommendations

The following recommendation to be done for further studies:

1. The synthesis and coating of ZnO with different metals such as Ag, Pd, Au.

2. Synthesized Cr_2O_3/ZnO nanocomposite by using green method.

3- Study the effect of nitrogen gas on the photocatalytc degradation process.

4- The photocatalytic studies using various electron scavengers like $KClO_3$, $KBrO_3$, KIO_4 and $K_2S_2O_8$ on decomposition of fuchsin acid dye.

5- The photocatalytic studies using electron scavenger and Cr_2O_3/ZnO nanocomposite photo catalyst on fuchsin acid dye .

References

References

- AbdulKareem, S.M., Suhail, M.H., Adehmash, K. (2021). Fabrication of Cr_2O_3: ZnO Nanostructure Thin Film Prepared by PLD Technique as NH3 Gas Sensor, Iraqi Journal of Science, pp: 2176-2187
- Abdulrazzak, H., Abed Jawad.M., Kamal.O., Alkaim.A. F. (2021) Antimicrobial Activity of Ag: ZnO\MWCNT against Acinetobacter baumannii. Journal of Nanostructures, (2): p. 317-322
- Abilarasu, A., Kumar, P. S., Vo, D. V. N., Krithika, D., Ngueagni, P. T., Joshiba, G. J., Prasannamedha, G. (2021). Enhanced photocatalytic degradation of diclofenac by SnO. 15MnO. 85Fe_2O_4 catalyst under solar light. Journal of Environmental Chemical Engineering, 9(1), 104875.
- Abu-Zurayk, R., Khalaf.A., Hussien Abbas.A., Rabab Nasr.A., Tarek Jamil.S and Abeer Al Bawab. (2021). Photodegradation of Carbol Fuchsin Dye Using an Fe2−xCuxZr2−xWxO7 Photocatalyst under Visible-Light Irradiation, Catalysts 2021, 11, 1473.
- Adya, A.K., Canetta.E.(2020). Nanotechnology and its applications to animal biotechnology. In Animal Biotechnology, Academic Press pp. 309-326
- Ainali, N. M., Kalaronis, D., Evgenidou, E., Bikiaris, D. N. Lambropoulou, D. A. (2021). Insights into biodegradable polymer-supported titanium dioxide photocatalysts for environmental remediation. Macromol, 1(3), 201-233.
- Akerdi, A.G., Bahrami.S.H.(2019). Application of heterogeneous nano-semiconductors for photocatalytic advanced oxidation of organic compounds: a review. Journal of Environmental Chemical Engineering, 7(5): p. 103283. 7

References

- Al-Gubury, H.Y., Altameme.H.J., Ali.M.M. (2018). Significant Enhancement of Photocatalytic Activity of Zinc Oxide Activity of Zinc Oxide by Extracted Anthocyanin Pigment and Solar Light. Plant Archives, 18(2), 2723-2726.
- Al-Gubury, Y.H., Karim.S.A., Abd Alrazzak.N. (2019, September). The synthesis of a novel azo dyes and study of photocatalytic degradation. In Journal of Physics: Conference Series (Vol. 1294, No. 5, p. 052054). IOP Publishing.
- Alkaç, I.M., Burcu.C.C., Timuralp.C.D., Fatih.S. A. (2021) Nanomaterials and their classification, in Nanomaterials for Direct Alcohol Fuel Cells., Elsevier. p. 17-33
- Alshehri, A., Narasimharao, K. (2020). PtOx-TiO_2 anatase nanomaterials for photocatalytic reformation of methanol to hydrogen: effect of TiO_2 morphology. Journal of Materials Research and Technology, 9(6), 14907-14921.
- Aziztyana, A. P., Wardhani, S., Prananto, Y. P., Purwonugroho, D. (2019). Optimisation of methyl orange photodegradation using TiO2-zeolite photocatalyst and H_2O_2 in acid condition. In IOP Conference Series: Materials Science and Engineering (Vol. 546, No. 4, p. 042047). IOP Publishing.
- Badvi, K., Javanbakht, V. (2021). Enhanced photocatalytic degradation of dye contaminants with TiO2 immobilized on ZSM-5 zeolite modified with nickel nanoparticles. Journal of Cleaner Production, 280, 124518.
- Barhoum, A., García-Betancourt.M.L., Jeevanandam.J., Hussien.E.A., Mekkawy.S.A., Mostafa.M., Bechelany.M. (2022). Review on natural, incidental, bioinspired, and engineered nanomaterials: history, definitions, classifications, synthesis,

properties, market, toxicities, risks, and regulations. Nanomaterials, 12(2), 177

- Benkhaya, S., M'rabet.S., El Harfi.A. (2020). A review on classifications, recent synthesis and applications of textile dyes. Inorganic Chemistry Communications, 115, 107891.
- Cai, M., Su.J., Zhu.Y., Wei.X., Jin.M., Zhan.H., Wei.Z. (2016). Decolorization of azo dyes Orange G using hydrodynamic cavitation coupled with heterogeneous Fenton process. Ultrasonics sonochemistry, 28, 302-310.
- Corrado, D., james.M., joseph.F.S., matthew. P. (2019) ZnO colloid crystal facet-type determines both Au photodeposition and photocatalytic activity. ACS Applied Nano Materials, p. 7856-7869
- Danyliuk, N., Tatarchuk, T., Shyichuk, A. (2020). Estimation of photocatalytic degradation rate using smartphone based analysis. Physics and Chemistry of Solid State, 21(4), 727-736.
- Dewil, R., Mantzavinos.D., Poulios.I., Rodrigo.M.A. (2017). New perspectives for advanced oxidation processes. Journal of environmental management, 195, 93-99.
- Erol, O., Uyan.I., Hatip.M., Yilmaz.C., Tekinay.A.B., Guler.M. O. (2018). Recent advances in bioactive 1D and 2D carbon nanomaterials for biomedical applications. Nanomedicine: Nanotechnology, Biology and Medicine, p.2433-2454.
- Fardood, S.T., Ramazani, A., Joo, S.W. (2018)., Green chemistry approach for the synthesis of copper oxide nanoparticles using tragacanth gel and their structural characterization, J. Struct. Chem, pp. 482-486
- Farghali, A.A., Zaki.A.H., Khedr.M.H. (2016). Control of selectivity in heterogeneous photocatalysis by tuning TiO_2

morphology for water treatment applications. Nanomaterials and Nanotechnology, 6, 12.

- Fu, J., Chen.Z., Wang.M., Liu.S., Zhang.J., Zhang.J., Xu.Q. (2015). Adsorption of methylene blue by a high-efficiency adsorbent (polydopamine microspheres): kinetics, isotherm, thermodynamics and mechanism analysis. Chemical Engineering Journal, 259, 53-61.
- Gholami, M., Shirzad-Siboni.M., Farzadkia.M., Yang.J.K. (2016). Synthesis, characterization, and application of ZnO\TiO_2 nanocomposite for photocatalysis of a herbicide (Bentazon). Desalination and water treatment, 57(29), 13632-13644.
- Hayat, K., Gondal.M.G., MKhaled.M., Ahmed.S., Shemsi.A.M.(2011). Nano ZnO synthesis by modified sol gel method and its application in heterogeneous photocatalytic removal of phenol from water. Applied Catalysis A: General, 393(1-2), 122-129.
- Imelda, E., Myriam.P., Roberto.M., Adriana.G., Guadalupe.S., Luisa M. Flores-Velez, Octavio Dominguez1, (2011), Solid State Reactions in Cr_2O_3-ZnO Nanoparticles Synthesized by Triethanolamine Chemical Precipitation, Materials Sciences and Applications, 2, 1584-1592
- Imran, M., Riaz, S., Shah, S. M. H., Batool, T., Khan, H. N., Sabri, A. N., Naseem, S. (2020). In-vitro hemolytic activity and free radical scavenging by sol-gel synthesized Fe_3O_4 stabilized ZrO_2 nanoparticles. Arabian Journal of Chemistry, 13(11), 7598-7608.
- Jadhav, A.S., Urkude.R.P., Jangam.S. S.(2021). CURRENT REVIEW ON NANOPARTICLES: PROPERTIES, APPLICATION AND TOXICITY, World Journal of Pharmaceutical Research,10(3),9001.

References

- Jamil, A., Bokhari, T. H., Javed, T., Mustafa, R., Sajid, M., Noreen, S., Jilani, M. I. (2020). Photocatalytic degradation of disperse dye Violet-26 using TiO_2 and ZnO nanomaterials and process variable optimization. Journal of Materials Research and Technology, 9(1), 1119-1128.
- Jamkhande, P.G., Ghule.N.W., Bamer.A.H., Kalaskar.M.G. (2019). Metal nanoparticles synthesis: An overview on methods of preparation, advantages and disadvantages, and applications. Journal of drug delivery science and technology, 53, 101174.
- Jones, N., B. Ray, K.T. Ranjit and A.C. Manna, (2008).Antibacterial activity of ZnO nanoparticle suspensions on a broad spectrum ofmicroorganisms. FEMS Microbiol. Lett., 279: 71-76.
- Kaiyuan, G.U., Zhanen Peng, Jinhua Feng and Fengqiang Sun. (2012). Preparation of ZnO-Cr_2O_3 Composites by a Sol-GelMethod and Their Photocatalytic Activities, Applied Mechanics and Materials Vol 151, pp 365-367
- Khan, I., Saeed.K. (2017). Nanoparticles: Properties, applications and toxicities. Arabian journal of chemistry, p.908-931 .
- Khan, I., Saeed.K., Ali.N., Zhang.B, Sadiq.M. (2020). Heterogeneous photodegradation of industrial dyes: an insight to different mechanisms and rate affecting parameters. Journal of environmental chemical engineering, 8(5), 104364.
- Kolahalam, L.A., Kasi.I., Viswanath, Diwakar.B.S., Govindh.B., Reddy.V, Murthy.Y.L. N. (2019). Review on nanomaterials: Synthesis and applications. Materials Today: Proceedings. 18: p. 2182-2190.
- Krishnakumar, B., Swaminathan.M. (2011). Influence of operational parameters on photocatalytic degradation of a

genotoxic azo dye Acid Violet 7 in aqueous ZnO suspensions. Spectrochimica Acta Part A: Molecular and Biomolecular Spectroscopy, 81(1), 739-744.

- Krishnan, T., Mansor.W.S.W. (2020). Photocatalytic Degradation of Dyes by TiO_2 Process in Batch Photoreactor. Letters in Applied NanoBioScience, 9, 1502-1512.
- Kumar, R., Janbandhu.S.Y., Sukhadeve.G.K., Gedam.R.S. (2022). Visible-light assisted surface plasmon resonance triggered Ag\ZnO nanocomposites: synthesis and performance towards degradation of indigo carmine dye. Research square
- Kumar, S., Kaushik.R.D., Purohit.L.P. (2021). Novel ZnO tetrapod-reduced graphene oxide nanocomposites for enhanced photocatalytic degradation of phenolic compounds and MB dye. Journal of Molecular Liquids, 327, 114814.
- Kzar, K.O., Mohammed.Z.F., Saeed.S.I., Ahmed.L.M., Kareem.D.I., Hadyi. H., Kadhim.A.J. (2019). Heterogeneous photo-decolourization of cobaltous phthalocyaninate dye (Reactive green dye) catalyzed by ZnO. In AIP Conference Proceedings (Vol. 2144, No. 1, p. 020004). AIP Publishing LLC.
- L. (2017). Acetone sensing of ZnO nanosheets synthesized using room-temperature precipitation. Sensors and Actuators B: Chemical, p. 611-623.
- Lee, S.C.., YJeong, Kim, Kim., LeeH.U., Lee.Y.C., Lee.G. (2018). Hierarchically three-dimensional (3D) nanotubular sea urchin-shaped iron oxide and its application in heavy metal re-moval and solar-induced photocatalytic degradation. Journal of hazardous materials, p. 3-292.

References

- Long, Z., Qiangang.L., Ting.W., Guangming.Z., Zhijun.R.(2020). Historical development and prospects of photocatalysts for pollutant removal in water. Journal of hazardous materials, 395: p. 122599.
- Maddu, A., Meliafatmah, R., Rustami, E. (2021). Enhancing Photocatalytic Degradation of Methylene Blue Using ZnO\Carbon Dots Nanocomposite Derived from Coffee Grounds. Polish Journal of Environmental Studies, 30(1).
- Madhavan, J., Grieser.F., Ashokkumar.M. (2010). Degradation of Orange-G by advanced oxidation processes. Ultrasonics sonochemistry, 17(2), 338-343.
- Mahdi, H. S., Ismael, K. A., Saadoon, M. Abdul Kareem· Dana, A. Tahir, Omed, Gh. Abdullah. (2020). Construction of Cr_2O_3: ZnO Nanostructured Thin Film Prepared by Pulsed Laser Deposition Technique for NO_2 Gas Sensor, Transactions on Electrical and Electronic Materials
- Makula, P., Pacia.M., macyk.W. (2018). How to correctly determine the band gap energy of modified semiconductor photocatalysts based on UV–Vis spectra. ACS Publications, Phys. Chem. 9, 6814−6817.
- Mamaghani, A.H., Haghighat.F., Lee.C.S.(2018). Hydrothermal\solvothermal synthesis and treatment of TiO2 for photocatalytic degradation of air pollutants: Preparation, characterization, p. S0045-6535
- Mancić, L., Marinković, Z., Vulić, P., Milosević, O. (2004). The Synthesis - Structure Relationship in the ZnO-Cr_2O_3 system, Science of Sintering, p. 189-196
- Marco, C., Giulio.F., Alberto.T., Minella.M., Vione.D. (2021). Advanced oxidation processes in the removal of organic substances

from produced water: Potential, configurations, and research needs, Chemical Engineering Journal 414 (2021) 128668

- Masuda, K., Kobayashi.S. (2020). Direct and quantitative monitoring of catalytic organic reactions under heterogeneous conditions using direct analysis in real time mass spectrometry. Chemical science, 11(19), 5105-5112.
- Meghdad, P., Shahmoradi.B., Masumeh.B.., esmaeel., Hooshyar.H, Ashraf.G.M.(2017). photocatalytic degradation of Aniline from aqueous solutions under sunlight illumination using immobilized Cr: ZnO nanoparticles, Scientific RepoRts | 7: 1473.
- Meng, L.S., Zhang.L.X., Meng.Y.Z., Guo.J.J., Zhao.X.L., Jing.Y., Jian.B.
- Meva, F.E., Ntoumba.A.A., Kedi.P. B, Tchoumbi.E., Schmitz.A., Schmolke.L., Janiak.C.. (2019) Silver and palladium nanoparticles produced using a plant extract as reducing agent, stabilized with an ionic liquid: sizing by X-ray powder diffraction and dynamic light scattering. Journal of Materials Research and Technology, 8(2), 1991-2000.
- Michael, C.J., Bradford, Mahesh Konduru.V., Digna.X.(2003), Preparation, characterization and application of Cr_2O_3\ZnO catalysts for methanol Synthesis, MA 02453, USA
- Mishra, V., Sharma.R. (2015). Green synthesis of zinc oxide nanoparticles using fresh peels extract of Punica granatum and its antimicrobial activities. International Journal of Pharma Research and Health Sciences, 3(3), 694-699.
- Mohamed, M. M., Ghanem, M. A., Khairy, M., Naguib, E., & Alotaibi, N. H. (2019). Zinc oxide incorporated carbon nanotubes or graphene oxide nanohybrids for enhanced sonophotocatalytic

degradation of methylene blue dye. Applied Surface Science, 487, 539-549.

- Mohamed, R.M., Adel, A. Ismail, Alhaddad, M. (2021). A novel design of porous Cr_2O_3@ZnO nanocomposites as highly efficient photocatalyst toward degradation of antibiotics: A case study of ciprofloxacin, Separation and Purification Technology 266 ,118588
- Mohammad, E.J., Lafta.A.J., Kahdem.S. E, & Alkaim.A.F. (2016). Enhancement the photocatalytic activity of zinc oxide surface by combination with functionalized and non-functionalized activated carbon. Int J ChemTech Res, 9(12), 656.
- Mohammad, R.K., Alireza, F., Homayon, A., Elaheh, K. (2021). Synthesis and characterisation of zinc oxide-chromium oxide for optimisation of photocatalytic/H_2O_2 process by response surface methodology: selective and regeneration studies, INTERNATIONAL JOURNAL OF ENVIRONMENTAL ANALYTICAL CHEMISTRY, p .1912331
- Mohsin, D.H., Juda.A.M., Mashkour.M. M. (2013). Thermodynamic and kinetic study for aromatic rings effect on the photooxidation rate. Int. J. Eng. Technol, 13, 34-41.
- Mondol, B., Sarker, A., Shareque, A. M., Dey, S. C., Islam, M. T., Das, A. K., Sarker, M. (2021). Preparation of activated carbon/TiO_2 nanohybrids for photodegradation of reactive red-35 dye using sunlight. Photochem, 1(1), 54-66.
- Mousavi, S.M., Behbudi.G., Gholami.G., Nejad.Z.M., Bahrani.S., Chiang.W.H. (2022) Shape-controlled synthesis of zinc nanostructures mediating macromolecules for biomedical applications. Biomaterials Research, p. 1-20.
- Mun Lam, S. JChung, S., Abdul Rahman, M. (2018) Cr_2O_3 Nanoparticles Anchored on ZnO Nanorods as Active Heterostructure Catalysts for Phenol Degradation, Sains Malaysiana, p. 253-259

References

- Nagabandi, J., Madhukar.P., Ramana.M.(2019). Enhanced Room Temperature Ammonia Gas Sensing Performance of ZnO-Cr_2O_3 Heterostructured Nanocomposites, AIP Conference Proceedings 2082, 030025.
- Nasrollahzadeh, M., Sajjadi.M., Soufi.G.J., Iravani.S., Varma.R.S., (2020). Nanomaterials and nanotechnology-associated innovations against viral infections with a focus on coronaviruses. Nanomaterials, 10(6), 1072.
- Neto, J. S.G., Satyro.S., Saggioro.E. M., Dezotti.M. (2021). Investigation of mechanism and kinetics in the TiO2 photocatalytic degradation of Indigo Carmine dye using radical scavengers. International Journal of Environmental Science and Technology, 18(1), 163-172.
- Niculescu, A.G., Grumezescu.A.M., (2022). Applications of Chitosan-Alginate-Based Nanoparticles—An Up-to-Date Review. Nanomaterials, 12(2), 186.
- Niu, B., Wu, D., Wang, J., Wang, L., Zhang, W. (2020). Salt-sealing-pyrolysis derived Ag/ZnO@ C hollow structures towards efficient photo-oxidation of organic dye and water-born bacteria. Applied Surface Science, 528, 146965.
- Olajire, A., Olajide.A. (2014). Kinetic study of decolorization of methylene blue with sodium sulphite in aqueous media: influence of transition metal ions , J Phys Chem Biophys, 2161-0398 JPCB
- Oun, A., Tahri.N., Mahouche-Chergui.S., Carbonnier.B., Majumdar.S., Sarkar.S., Amar.R.P. (2017). Tubular ultrafiltration ceramic membrane based on titania nanoparticles immobilized on macroporous clay-alumina support: elaboration, characterization and application to dye removal. Separation and Purification Technology, 188, 126-133.

References

- Pimentel, A., Rodrigues.J., Duart.P., Nunes.D., Costa.F.M., Monteiro.T., Martins.R., Fortunato.E.(2015). Effect of solvents on ZnO nanostructures synthesized by solvothermal method assisted by microwave radiation: A ph. otocatalytic study. Journal of Materials Science, p. 5777-5787.
- Prasad, A.R., Williams.L., Garvasis.J., Shamsheera.K.O., Sabeel.M.B., Mathew.K., Abraham.J. (2021). Applications of phytogenic ZnO nanoparticles: A review on recent advancements. Journal of Molecular Liquids, 331: p. 115805
- Qixuan,Q., SHEN,Z., ZHANG, N.,ZHANG, X.(2011). Design of Cr2O3@ZnO Hetero-junction Hierarchical Nanostructures with Enhanced Xylene-sensing Properties, 40242-018
- Rajput, V.D., Minkina.T., Fedorenko.A., Chernikova.N., Hassan.T., MandzhievaS., Burachevskaya.M. (2021). Effects of zinc oxide nanoparticles on physiological and anatomical indices in spring barley tissues. Nanomaterials, 11(7), 1722.
- Rashid, A., Bhatti, H. N., Iqbal, M., Noreen, S. (2016). Fungal biomass composite with bentonite efficiency for nickel and zinc adsorption: a mechanistic study. Ecological engineering, 91, 459-471.
- Reda, M., Adel ,A., Maha ,A.(2021). A novel design of porous Cr2O3@ZnO nanocomposites as highly efficient photocatalyst toward degradation of antibiotics: A case study of ciprofloxacin, Separation and Purification Technology 266 (2021) 118588.
- Resmi, R., Yoonus, J., Beena, B. (2021). A novel greener synthesis of ZnO nanoparticles from Nilgiriantusciliantus leaf extract and evaluation of its biomedical applications. Materials Today: Proceedings, 46, 3062-3068.
- Rhazouani, A., Gamrani.H., Achaby.M.E., Aziz.K., Gebrati.L., Uddin, M. S., F. Aziz, (2021). Synthesis and toxicity of graphene

oxide nanoparticles: A literature review of in vitro and in vivo studies. BioMed Research International, p.19

- Saleh, T. A. (2020). Nanomaterials: Classification, properties, and environmental toxicities. Environmental Technology & Innovation p. 101067
- Salma A. Al-Zahrani, Mallikarjunagouda B., Shridhar N. Mathad, Arun Y. Patil, Ahmed A. Otaibi, Najat Masood, Dorsaf Mansour, Anish Khan, A. Manikandan and Edi Syafri. (2023). Photocatalytic Degradation of Textile Orange 16 Reactive Dye by ZnO Nanoparticles Synthesized via Green Route Using Punica Granatum Leaf Extract, Crystals, p.172
- Samsudin, E.M., Goh.S.N., Wu.T.Y., Ling.T.T., Hamid.S.A., Juan.J.C. (2015). Evaluation on the photocatalytic degradation activity of reactive blue 4 using pure anatase nano-TiO_2. Sains Malaysiana, 44(7), 1011-1019.
- Sang, W.P., Oh-Shim Joo, Kwang-Deog Jung, Hyo Kim and Sung-Hwan Han, (2000). $ZnO\backslash Cr_2O_3$ Catalyst for Reverse-Water-Gas-Shift Reaction of CAMERE Process, Korean J. Chem. Eng., 17(6), 719-722.
- Saratale, R.G., Saratale.G.D., ChangJ.S., Govindwar.S.P. (2011). Bacterial decolorization and degradation of azo dyes: a review. Journal of the Taiwan institute of Chemical Engineers, 42(1), 138-157.
- Sharma, A., Ahmad.J., Flora.S. (2018). Application of advanced oxidation processes and toxicity assessment of transformation products. Environmental research, 167, 223-233.

References

- Sharma, P. K., & Pandey, O. P. (2021). Effect of processing parameters on structural and optical properties of CeO_2 nanoparticles for the removal of crystal violet dye. Journal of Sol-Gel Science and Technology, 99(1), 75-91.
- Shashanka, R., Parham, T., Abdullah, C. Karaoglan Shashanka Rajendrachari, Parham Taslimi, Abdullah Cahit Karaoglanli, Orhan Uzun, Emre Alp, Gururaj Kudur Jayaprakash li, Orhan, U., Emre Alp, Gururaj Kudur Jayaprakash. (2021). Photocatalytic degradation of Rhodamine B (RhB) dye in waste water and enzymatic inhibition study using cauliflower shaped ZnO nanoparticles synthesized by a novel One-pot green synthesis metho, Arabian Journal of Chemistry, p103180
- Sicong, M.A., Si-Da Huang, Zhi-Pan Liu, (2019), Dynamic coordination of cations and catalytic selectivity on zinc–chromium oxide alloys during syngas conversion, Nature Catalysis,2, 671–677.
- Singh, A., Chahal, S., Dahiya, H., Goswami, A., & Nain, S. (2021). Synthesis of Ag nanoparticle supported graphene\multi-walled carbon nanotube based nanohybrids for photodegradation of toxic dyes. Materials Express, 11(6), 936-946.
- Suhail, M.H., Adehmash.I.K., Abdul Kareem.S.K., Tahir.D.A., Abdullah.O.G.(2020). Construction of Cr_2O_3: ZnO Nanostructured Thin Film Prepared by Pulsed Laser Deposition Technique for NO_2 Gas Sensor, Electrical and Electronic Material Engineers, 2092-7592
- Sundar, K.P., Kanmani.S.(2020). Progression of Photocatalytic reactors and its comparison, A Review. Chemical Engineering Research and Design, 154: p. 135-150

References

- suresh babu, K., nayaranan. V. (2013). Hydrothermal Synthesis of Hydrated Zinc Oxide Nanoparticles and its Characterization, Department of Inorganic Chemistry, University of Madras, Guindy Campus, Chennai-600025, India, p. 33-36
- Suresh, G., Shreyas.P., Mohammed.B., Shirish.S., Rajeshware.O.(2021). Environmentally friendly synthesis of Cr_2O_3 nanoparticles: Characterization, applications and future perspective ─ a review, Case Studies in Chemical and Environmental EngineeringVolume 3, June 2021, 100089
- Sze-Mun, L., Jin-Chung, S., Abdul Rahman. M. (2018). Cr_2O_3 Nanoparticles Anchored on ZnO Nanorods as Active Heterostructure Catalysts for Phenol Degradation, Sains Malaysiana, p: 253-259
- Wang, Z., Hu.T., Liang.R., Wei.M. (2020). Application of zero-dimensional nanomaterials in biosensing. Frontiers in Chemistry, 8, 320.
- Wani,S.,I., Ganie,A.,S.(2021). Ag_2O incorporated ZnO − TiO_2 nanocomposite: Ionic conductivity and photocatalytic degradation of an organic dye, Inorganic Chemistry Communications 128 (2021) 108567
- Weldegebrieal, G.K. (2020). Synthesis method, antibacterial and photocatalytic activity of ZnO nanoparticles for azo dyes in wastewater ltreatment: A review. Inorganic Chemistry Communications, 120: p. 108140
- Worasawata,S., Tomoaki, M., Yoshinori, H. , Yoichiro, N., Hidenori, M.,Wisanu, P.(2018)
- Yang, G., Park.S. J. (2019) Conventional and microwave hydro-thermal synthesis and application of functional materials: A review. Materials, p. 1177.

References

- Ye, N., Yan.T., Jiang.Z., Wu.W., Fang.T.(2018). A review: conventional and supercritical hydro\solvothermal synthesis of ultrafine particles as cathode in lithium battery. Ceramics International, p. 4521-4537.
- Zelekew, O.A., Paulos Asefa Fufa., Fedlu Kedir Sabir., Alemayehu Dubale Duma. (2021). Eichhornia crassipes plant extract templated green synthesis of Cr_2O_3/ZnO composite catalyst for the degradation of organic dye, A: chemistry, p. 110 – 118
- Zelekew, O.A., Paulos.A.F., Fedl.K.S., Alemayehu.D.D.(2021) Water hyacinth plant extract mediated green synthesis of Cr_2O_3\ZnO composite photocatalyst for the degradation of organic dye, materals science, e07652
- Zhang, L., Y. Jiang, Y. Ding, N. Daskalakis and L.Jeuken et al., (2010). Mechanistic investigation into antibacterial behaviour of suspensions of ZnO nanoparticles against *E. coli*. J. Nanoparticle Res.,12: 1625-1636.
- Zhao, J., Tiana.Y., Liua.A., Songb.L., Zhaoa.Z. (2019). The NiO electrode materials in electrochemical capacitor: A review. Materials Science in Semiconductor Processing, p. 78-90.
- Zhenzhao, P., Xianlong, Z., and Zhiguo L. (2016). Progress on Synthesis and Applications of Cr_2O_3 Nanoparticles, Journal of Nanoscience and Nanotechnology p. 4655–4671

الخلاصة :

تحتوي هذه الرسالة على جزئين رئيسيين:

يتضمن الجزء الأول تحضير جزيئات أكسيد الزنك (ZnO) النانوية بطريقة التخليق الحراري المائي وتحضير المتراكب النانوي Cr_2O_3/ZnO بطريقة التخليق الحراري المائي. دراسة خصائص المركبات النانوية باستخدام تقنيات مختلفة مثل حيود الأشعة السينية (XRD)، للأشعة تحت الحمراء (FTIR)، والمسح المجهري الإلكتروني (SEM)، والحرارة تحليل الجاذبية (TGA). تم حساب حجم البلوري للمتراكب النانوي Cr_2O_3/ZnO باستخدام معادلة شيرر (12.72 نانومتر).

الجزء الثاني يتضمن دراسة النشاط التحفيزي الضوئي لمركب النانو المحضر باستخدام صبغة fuchsin الحامضية. يتم دراسة تأثر مجموعة من العوامل المؤثره على عملية التكسير الضوئي مثل التركيز الأولي للصبغة، وتأثير كتلة المحفز، ودرجة الحموضة الأولية للمحلول، وتأثير درجة الحرارة، وتأثير المواد المثبطه لعملية التكسير الضوئي وتاثير بيروكسيد الهيدروجين يتضمن أفضل نسبة إزالة صبغة fuchsin ال حامضية(85.23%). تم دراسة تأثير تركيز الصبغة على القيمة المثلى لصبغة fuchsin الحامضية)mg / L 20). الرقم الهيدروجيني = 9 ودرجة الحرارة 25 درجة مئوية وفي ظروف المختبر لصبغة fuchsin الحامضية. تم حساب طاقة التنشيط لعملية التحلل الضوئي باستخدام معادلة أرينيوس حيث كانت تساوي (31.67 كيلوجول/ مول) وتم تقدير التغير بدالة الانثالبي والانتروبي والتغير بدالة الطاقة الحره وفقًا لمعادلة ايرنك. تم حساب الدوال الديناميكية الحرارية (ΔH، ΔS، ΔG) لصبغة fuchsin الحامضية (29.20 كيلوجول / مول و - 0.1778 كيلوجول / مول. كلفن) على التوالي، من النتائج يكون التفاعل ماصًا للحرارة مع عشوائية منخفضة. تم حسابΔG (82.18. كيلوجول / مول).

جمهورية العراق

وزارة التعليم العالي والبحث العلمي

كلية العلوم للبنات \ جامعة بابل

قسم الكيمياء

التخليق الحراري المائي للمتراكب النانوي $Cr_2O_3\backslash ZnO$ للتطبيقات البيئية

رسالة مقدمة إلى
مجلس كليـــة العلوم للبنات في جامعـــة بابـــل وهي
جـزء من متطلبات نيل درجـــة الماجستير
في الكيمياء

رسالة مقدمة من قبل

كرم كاظم عبدزيد جواد الشريفات

بأشراف

أ. د حازم يحيى محمد علي

2023م **1444ه**